UNIVERSITÀ DEGLI STUDI DI SALERNO

DIFARMA

UNIVERSITÀ DEGLI STUDI DI SALERNO

Dipartimento di Farmacia

PhD Program
in **Drug Discovery and Development**

XXXIV Cycle – Academic year 2021/2022

Ph.D. thesis in

Design, Synthesis, and characterization of peptides from Gp36 FIV glycoprotein

Candidate

Mohammad Firoznezhad

Supervisor

Prof. *Anna Maria D'Ursi*

Ph.D. Program Director: Prof. *Gianluca Sbardella*

List of publications

[1] Buonocore, M., Marino, C., Grimaldi, M., Santoro, A., **Firoznezhad, M.**, Paciello, O., ... & D'Ursi, A. M. (2020). New putative animal reservoirs of SARS-CoV-2 in Italian fauna: A bioinformatic approach. Heliyon, 6(11), e05430.

[2] Covelli, V., Grimaldi, M., Randino, R., **Firoznezhad, M.**, Proto, M. C., Simone, V. D., ... & Rodriquez, M. (2021). Towards an Improvement of Anticancer Activity of Benzyl Adenosine Analogs. Molecules, 26(23), 7146.

Preface

My Ph.D. in Drug Discovery and Development began in November 2018 at the Department of Pharmacy of Salerno University, under the supervision of Professor Anna Maria D'Ursi.

My Ph.D. research was focalized on the study of the Design, synthesis, and characterization of peptides from Gp36 Feline Immunodeficiency Virus glycoprotein.

The research activity focused on C8, an octapeptide belonging to the MPER region of gp36 endowed with significant anti-FIV activity. Part of my activity was focused on exploring the possibility that C8 may be used to favor differentiation of neuronal cells and thus in tissue engineering and regeneration. Then in the attempt of identifying C8 analogs endowed with improved pharmacodynamic and pharmacokinetic properties, I synthesized new C8 analogs characterized by restricted conformational properties and non-natural aminoacid substitution. Finally, I performed NMR conformational analysis of a peptide belonging to the NH region of gp36 that is known to exert inhibitory activity with respect to C8.

The entire work was carried out under the direct supervision of Prof. Anna Maria D'Ursi. Furthermore, to improve my knowledge on epitope mapping and synthesis of different peptide analogs with different techniques, I spent a period of research activity at the University of Copenhagen (Department of Drug Design and pharmacology under the supervision of Prof.Paul Robert Hansen, Prof.Michael Gajhede and prof.Peter Waaben Tholstrup.

Table of contents

Abstract

Glycoproteins gp36 in FIV and gp41 in Human Immunodeficiency Virus (HIV) promote the fusion of virus envelope with the host cell membranes. They have a similar framework that includes the fusion peptide (FP), N-terminal heptad repeat (NHR), C-terminal heptad repeat (CHR), and membrane-proximal extracellular region (MPER). MPER is a hydrophobic, Trp-rich region characterized by a significant bio-membrane affinity. Virus entry is effective once NHR and CHR fold back to form a low-energy, stable six-helical bundle (6HB). MPER plays a significant role during this process by correctly driving the virus membrane to assemble with the host cell membrane.

FIV and HIV entry can be efficiently inhibited by peptides mimicking conserved functional elements of Gp41 or Gp36. A prominent example of such peptides, termed fusion inhibitors, is the peptide T-20 (enfuvirtide, Fuzeon), which is used as salvage therapy for HIV/AIDS.

We previously identified C8, a peptide belonging to the Gp36 MPER, that exhibited significant anti-FIV activity in vitro and in vivo. Extensive biophysical investigation indicated an unusual ability of C8 in interacting with phospholipid membrane and evidenced that the adsorption of C8 on the membrane causes membrane remodeling, with the formation of membrane "nipples" and tubes to create a tight network of membrane connections.

Starting from these data, part of my Ph.D. research activity explored the possibility that the activity of C8 at the membrane level can be valuably used to promote cell differentiation and tissue regeneration. Therefore I produced C8 functionalized polycaprolactone (PCL) scaffolds and evaluated the ability of these devices to affect SH-SY5Y neuronal cells. Our data show that PCL can be efficiently functionalized with C8, and these scaffolds are efficient in promoting cell proliferation with modification of their shapes. In particular, PCL C8 functionalization induces better cell adhesion and spreading on the fiber surface, evidencing the ability to

improve interaction with the material.

The rational design of peptides capable of inhibiting the formation of 6HB in Gp36 takes advantage of structural information on the fragments that may interact with each other. Specifically, it would be advantageous to understand how in the Gp36 six-helix bundle TM interacts with FP, NHR with CHR, and PR with MPER. To collect this information, in addition to C8, we previously solved the NMR structure of a construct including the full MPER, and part of the CH region. Extending this structural investigation, part of my Ph.D. activity was focused on studying the NMR structure of C20 -a peptide corresponding to the sequence 627-646 of Gp36 NHR- that proved to inhibit C8 activity. Our data show the preference of C20 to assume a regular α-helix in the central part of the sequence. Furthermore, molecular dynamics calculation indicates that C20 forms a stable structural complex with CH-MPER, establishing interactions mainly with the CHR portion.

Finally, in the context of identifying C8 analogs endowed with improved inhibitory activity and pharmacokinetic properties, my research experience at the University of Copenhagen, under the supervision of Prof.Paul Robert Hansen, was focused on i) the synthesis of new C8 analogs. Based on the idea that reducing the conformational flexibility may improve the biological activity of short peptides, I synthesized a cyclic analog of C8 by performing a tail-to-head cyclization of linear C8. On the other hand, in view of the critical role played by Trp residues in the C8 sequence, I synthesized C8 analogs, including tryptamine residues in place of Trp residues. The biological activity of these compounds is under investigation.

2) Identifying new sequences belonging to Gp36 capable of interfering with the formation of the six-helix bundle. Gp36 epitope map scanning was performed using molecular docking to identify the GP36 decapeptide sequences capable of an optimized interaction with the whole Gp36 protein. A set of 33 peptide sequences was screened vs. a Gp36 structure built by homology modeling using as template Gp41 crystal coordinates. Molecular docking screening points to four peptide sequences characterized by optimal docking score and energetic

parameters. These were synthesized by standard solid-phase synthesis protocols and are currently under investigation to evaluate their antiviral properties.

1 Introduction

Human immunodeficiency virus (HIV) is the causative agent of acquired immunodeficiency syndrome (AIDS), a syndrome characterized by a series of severe infections caused mainly by opportunistic microorganisms and particular neoplastic manifestations (Kaposi's sarcoma, lymphoma) secondary to severe immunodeficiency.

HIV is a pathogenic retrovirus belonging to the Retroviridae family and the Lentivirus genus,. Its genome comprises two RNA molecules (it is therefore a ribo-virus), which are not translated directly during the replication cycle. An enzyme called reverse transcriptase transcribe it into many DNA molecules (provirus), which can integrate into the host cell genome.

The generic name HIV is used to refer to two different types of viruses:

- HIV-1, the most widespread type responsible for the AIDS epidemic in Italy and in the rest of Europe, the United States and Central Africa.

- HIV-2: it is most common in West Africa, South America and the Caribbean.

HIV is very similar to feline immunodeficiency virus (FIV), another Lentivirus infecting domestic cats (Felis catus), pumas (Puma concolor), lions (Panthera leo) and leopards (Panthera pardus).[1]

HIV has been widely studied: characterized by a 100-120 nm diameter, it shows an icosahedral structure including the envelope (pericapsid), the matrix (capsid), and the nucleus (nucleocapsid). The envelope surrounds the virus from the outside and consists of a phospholipid bilayer derived from the host cell's cytoplasmic membrane.[2]

Viral glycoproteins surround the envelope, gp120 (SU), a surface protein with anti-receptor function, and gp41 (TM), a transmembrane protein with fusogenic activity, both derived from the proteolytic cleavage of gp160 (product of the viral env gene) and involved in virus-host cell interaction. gp41 is more directly involved in the fusion process of the virus with the host cell and lies below gp120, folded towards the hydrophobic layer of the phospholipid membrane. The function of these proteins is to help the virus recognize, bind, and invade host cells.

1.1 FIV

FIV belongs to the Retroviridae family, genus Lentivirus, and was first isolated in California in 1987.[3] It is a lentivirus infecting domestic cats; it is not transmissible to humans, shares many biological and physio-pathogenic characteristics with HIV.

Despite tremendous progress in this field, there is still no cure or vaccine for HIV.[4] Therefore, identifying an appropriate animal model is essential to improve the knowledge of this pathogen. FIV and its natural host, the domestic cat, are particularly suitable among the various available models. This is because, despite the phylogenetic distance from HIV-1, there are similarities in the genomic organization, morphological structure, biological properties, and persistence of infection in the natural host.[5]

FIV has a worldwide distribution. Transmission occurs primarily through bite wounds and is common in male cats who live outdoors or leave their homes. The virus is not characterized by high contagiousness and infection. In nature, it occurs in three to four clinical stages, which differ from each other in terms of symptomatology, duration, and impairment of the immune system.

The first stage of the disease has an incubation period of about a month; it causes fever, lethargy, and more or less marked enlargement of the lymph nodes and may last for weeks or even months. After this initial clinical phase, cats become symptomatic carriers that enter the latency phase for a very long, variable period (even 3 years), without showing clinical signs, but at the same time showing a progressive decline in immune defenses. As with HIV, FIV infects CD4+ T cells. FIV-infected cats show a marked decrease in immune defenses, making them susceptible to other pathogens. The final stage of pathology is characterized by a rapid decline in the cat's general condition, leading to death. Similar to HIV and other lentiviruses, the surface glycoprotein of FIV gp45 (analogous to gp120 of HIV) and the transmembrane glycoprotein gp36 (analogous to gp41 of HIV), encoded by the env gene, play critical roles in the early stages required for the virus to enter the cell. They are considered the primary target for the immune response.

The discovery of FIV as the cause of a syndrome similar to that caused by HIV-1 in humans has highlighted the potential of this lentivirus as a model for the study of AIDS.[6] Because HIV-1 does not replicate in nonhuman cells, it has become necessary to use lentivirus animal host models to study infection in vivo and to analyze aspects of the biology of the virus in order to develop potential therapeutic strategies and vaccines. Although none of the available animal models are the exact counterpart of HIV-1 infection in humans, the FIV/domestic cat system has many advantages that make it suitable for this type of study. Other similarities of this virus with the human one includes the replicative cycle, the in vitro cytopathic effect, and the tropism for macrophages and T lymphocytes. For these reasons, FIV has been and continues to be studied to investigate specific aspects relative to lentiviral pathogenesis and to develop antiviral drugs and therapies.

Concerning this last point, FIV has been used successfully for the development of ex vivo active protease inhibitors against FIV, HIV-1 and SIV.[1] The FIV/cat model is also particularly attractive in developing vaccination strategies against HIV-1. In this regard, a model advantage is that FIV, like HIV-1, has several viral subtypes, a characteristic that allows to test the effectiveness of vaccines against heterologous challenges.[2] Furthermore, FIV is a good model for developing safe vector systems to transduce specific cells into different organs and tissues.[3] Eventually, other interesting aspects of FIV are its species specificity, which reduces the risk of infection for laboratory workers who manipulate this virus, and the low costs of purchasing and managing animals.

1.2 Viral surface glycoproteins: gp41 and gp36

1.2.1 gp41 structure

As mentioned above, the surface glycoprotein of FIV, gp45, corresponds to gp120 of HIV, and gp36, a transmembrane glycoprotein, corresponds to gp41 of HIV. These glycoproteins play a critical role in the early stages necessary for the virus to enter the cell and are considered primary targets for the immune response and the development of anti-FIV therapeutics.[6-8]

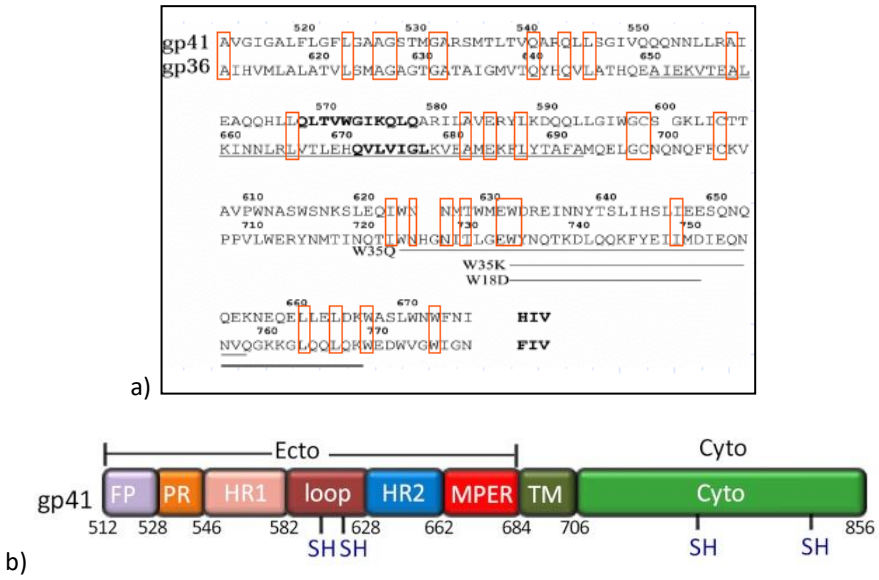

Figure 1. a) Structure positioning between gp41(HIV) and gp36(FIV) carried out by the CLUSTALW algorithm. b) Schematic representation of HIV gp41. The diverse parts are mentioned with abbreviation: Ecto (ectodomain); FP (Fusion Peptide); PR (Fusion Peptide proximal region); HR1(Heptad Region1 or N' heptad Region); HR2 (Heptad Region 2 or C' heptad region); MPER (Membrane Proximal External Region); TM (Transmembrane Region); Cyto (Cytoplasmic tail).

Alignment of the sequences of gp41 and gp36 shows (**Figure 1a**) a high degree of homology with a common structural architecture as follows (**Figure 1b**):

- Fusion peptide (FP), a hydrophobic area rich in glycine residue, referring to the first 15 aa, followed by the proximal region (PR). These regions induce cell membrane destabilization.
- *Heptad Region 1* (HR1) or N heptad repeat (NHR), and *Heptad Region 2* (HR2) or C heptad repeat (CHR) at the C-terminal. The NHR and CHR regions bind each other to form α-helical coiled coils,[7] which are necessary for the fusion process of the virus with the host cell.

- Hydrophobic loop of 25-30 residues with two cysteines forming a disulfide bridge.
- Transmembrane domain (TM), consisting of 22 amino acids, largely conserved region.
- Cytoplasmic domain (CP), consisting of about 150 amino acids endowed with important functions *in vivo*.
- Membrane proximal external region (MPER), located between the CHR and TM domain, rich in Trp residues. It promotes the adhesion of the glycoproteins to the lipid membranes.

1.2.2 Role of gp41 in the fusion process

The interaction of gp45 (gp120 in HIV) with the CD4 receptor and CXCR4, a chemokine co-receptor, causes a conformational change of gp36 (gp41 in HIV) from a native state to an intermediate state before melting to an active fusion state (**Figure 2**).

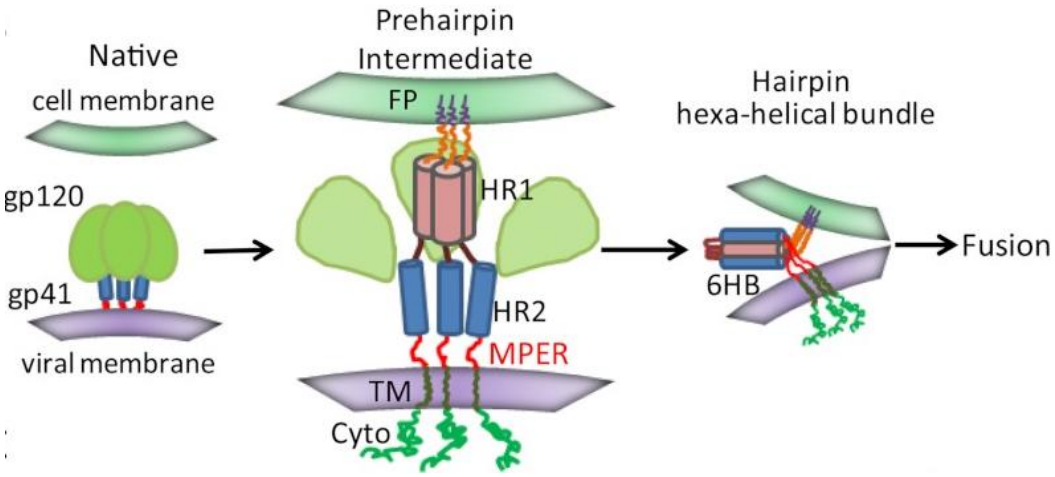

Figure 2. Schematic representation of the fusion process mediated by gp41.

In the initial state, gp41 and gp120 are linked together so that the fusion peptide is hidden inside the *envelope*. In the pre-fusion or intermediate state, the N-terminal appears as a trimeric coiled-coil with a parallel helix. The amino-terminal hydrophobic fusion peptide, located at the tip of the N-peptide helix of the ectodomain, is introduced into the target cell membrane and exposes the NHR and CHR regions, initiating the fusion process; the C-peptide region, however, is anchored to the viral membrane by a transmembrane segment.

In the fusion state, the NHR and CHR regions form a six-helical bundle (hairpin structure) are known as the "trimeric core of antiparallel heterodimers" of the gp41 ectodomain or "hairpin trimer."

This conformational state is critical for the viral and cellular membranes to converge, culminating in the release of the nucleocapsid into the cytoplasm.[7, 8]

1.2.3 MPER region

MPER, an acronym for the membrane-proximal external region, is a hydrophobic region containing ~24 residues (residues 660-683) that immediately precedes the transmembrane domain (TM) and is one of the most conserved regions in lentivirus glycoproteins.[9-11]

MPER is rich in aromatic residues, particularly Trp, and shows a marked tendency to remain permanently at the membrane interface, leading to destabilization of the bilayer structure of the target cell. Many studies have shown that removal or replacement of this region disturbs the fusogenic action of viral glycoproteins and avoids viral entry into the host cell.[12] Indeed, mutations of the first three Trp (Trp^{666}, Trp^{670}, Trp^{672}) are necessary to prevent viral fusion.

It has been proposed that MPER activity at the membrane interface occurs through membrane protrusions rich in cholesterol (Chol) and sphingomyelin (SM). This passage requires the major energy barrier that must be overcome to the initiate fusion between membranes.[13]

Peptides derived from the MPER domain of gp41 and gp36 have been extensively studied

to develop anti-FIV or anti-HIV therapeutics that can inhibit the fusion of HIV or FIV with host cell membranes.[14-18]

Moreover, the MPER region contains epitopes that stimulate immune responses and can be recognized by specific monoclonal antibodies. For this reason, these domains of gp36 and gp41 are considered important targets for vaccine development.[9-11, 19]

1.3 Identification of antiviral peptide C8

Gp41 and Gp36 conformational rearrangement can be efficiently inhibited by peptides mimicking their functional elements. A prominent example of such peptides, termed fusion inhibitors, is the peptide T-20 (enfuvirtide, Fuzeon), used as salvage therapy for HIV/AIDS.[13]

In a similar experimental approach, we previously identified C8, a peptide belonging to the Gp36 MPER that exhibited significant anti-FIV activity in vitro and in vivo. Therefore, in an attempt to design anti-FIV analogous of C8, a strand of our laboratory research has focused over the year on the study of C8 with regard to i) study of structure-activity relationship; ii) study of its mechanism of action, and biophysical behavior on membranes of biological interest, iii) the study of an extended region of its parent peptide MPER corresponding iv) the study of molecules belonging to Gp36 and potential interferents of C8 action.[13-17, 20]

1.4 C8 biophysical: properties

Extensive structure-activity relationship studies showed that Trp residues at a correct distance are critical for anti-FIV activity. The correct orientation of Trp side chains is also critical, as demonstrated by C8 retro-inverso analog preserving the biological activity of its present peptide (**Figure 3**).[21]

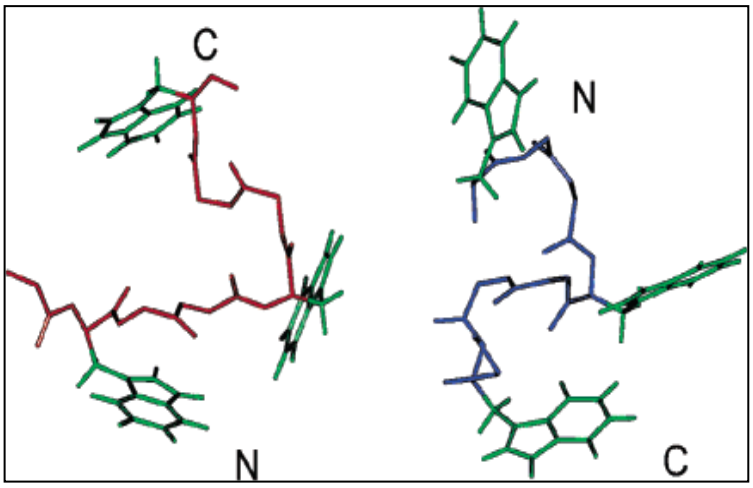

Figure 3. C8 (right) and riC8 (left) structures.

The conformation of C8 was studied in micelle solution using NMR spectroscopy. (**Figure 4**).[22] The best NMR conformation is characterized by type-I β-turn conformations with indole rings of Trp^{770} and $Trp^{773,}$ forming a hydrophobic coat that interacts with the surface of micelles.[22]

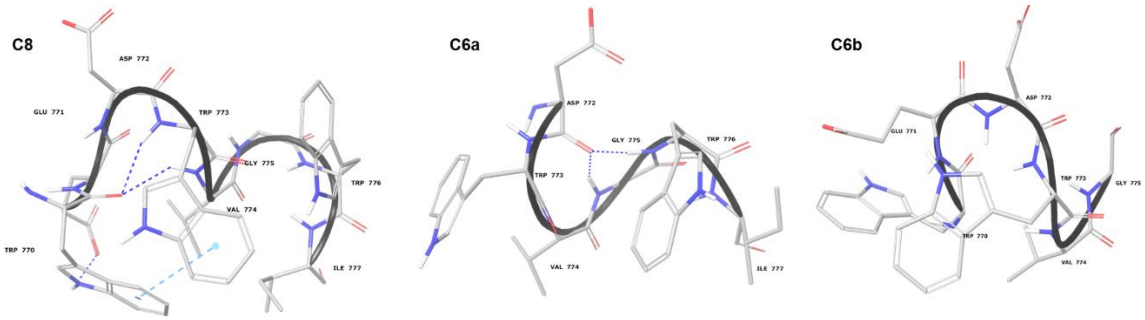

Figure 4. Low energy NMR models calculated for C8, C6a and C6b peptides in DPC/SDS 90:10 molar ratio.

Numerous data have shown that the antiviral effect of C8 is related to its interaction with the host cell membrane to prevent access to FIV.[14] To investigate the details of this mechanism, C8 has been studied in several different membrane-mimicking systems using spectroscopy combined with molecular dynamics simulations (**Figure 5**). These studies showed that hydrogen bonds and hydrophobic interactions involving the Trp indole control the binding of C8 to the lipid bilayer. Binding to the membrane leads to a local decrease in the bilayer thickness with hydration of the lipid head groups 35, culminating in a reorganization of the phospholipid

bilayer.[23-25]

Analysis performed with confocal microscopy imaging shows that the effect observed on the membrane with molecular dynamics, can be the first step of a process leading to the formation of membrane nipples and tubes to form a straight network of membrane tubulation.[26, 27]

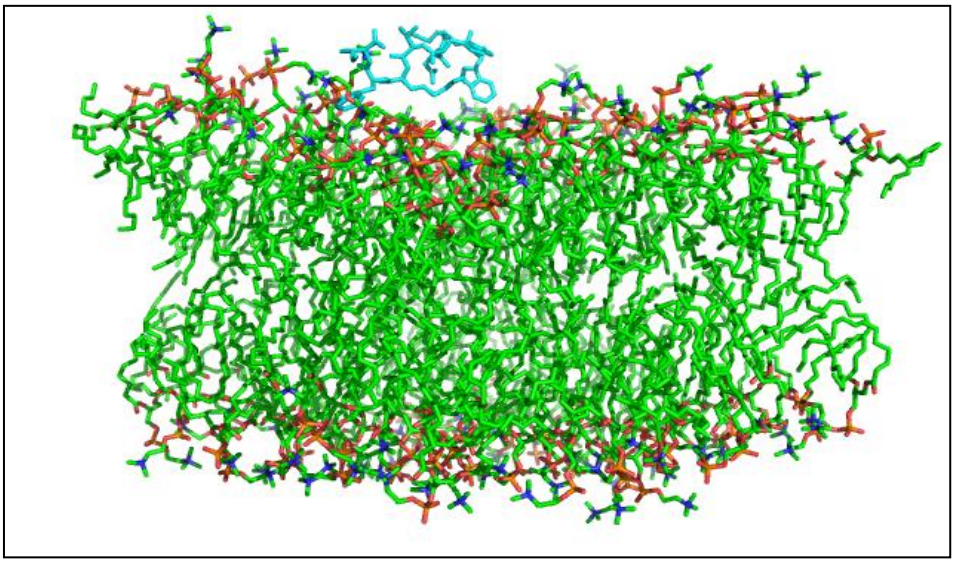

Figure 5. Interaction model of C8 peptide (in light blue) with lipid double layer surface (in green)[28]

To study C8 in even more biomimetic systems, we turn to study vesicles deriving from cells in response to external stress.[24, 29] [19, 30-33] Confocal microscopy imaging shows that C8 perturbs the system, enhancing cell-derived vesicles' movement in these systems. As a result, they rapidly allineate themselves to form a collar and merge to form straight tubular networks.[26]

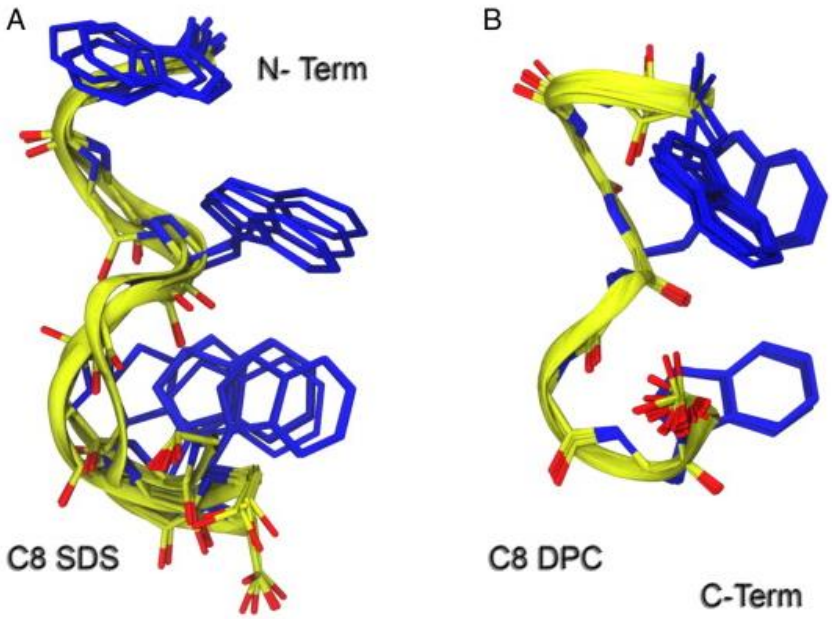

Figure 6. NMR structure of C8 peptide in micelle solutions of SDS (A) and DPC (B). The structures have been superimposed on the backbone level. The display mode was adopted using a stick and the side chains of Trp^{770}, Trp^{773} and Trp^{776} were highlighted in blue.[34]

1.5. References

1. Elder, J.H., et al., *Molecular mechanisms of FIV infection.* Vet Immunol Immunopathol, 2008. **123**(1-2): p. 3-13.
2. Dunham, S.P., *Lessons from the cat: development of vaccines against lentiviruses.* Vet Immunol Immunopathol, 2006. **112**(1-2): p. 67-77.
3. Sauter, S.L. and M. Gasmi, *FIV vector systems.* Somat Cell Mol Genet, 2001. **26**(1-6): p. 99-129.
4. Giannecchini, S., et al., *The membrane-proximal tryptophan-rich region in the transmembrane glycoprotein ectodomain of feline immunodeficiency virus is important for cell entry.* Virology, 2004. **320**(1): p. 156-66.
5. Salzwedel, K., J.T. West, and E. Hunter, *A conserved tryptophan-rich motif in the membrane-proximal region of the human immunodeficiency virus type 1 gp41 ectodomain is important for Env-mediated fusion and virus infectivity.* J Virol, 1999. **73**(3): p. 2469-80.
6. Suárez, T., et al., *Membrane interface-interacting sequences within the ectodomain of the human immunodeficiency virus type 1 envelope glycoprotein: putative role during viral fusion.* J Virol, 2000. **74**(17): p. 8038-47.
7. Chambers, P., C.R. Pringle, and A.J. Easton, *Heptad repeat sequences are located adjacent to hydrophobic regions in several types of virus fusion glycoproteins.* J Gen Virol, 1990. **71 (Pt 12)**: p. 3075-80.
8. Chan, D.C. and P.S. Kim, *HIV entry and its inhibition.* Cell, 1998. **93**(5): p. 681-4.
9. Muster, T., et al., *A conserved neutralizing epitope on gp41 of human immunodeficiency virus type 1.* J Virol, 1993. **67**(11): p. 6642-7.
10. Stiegler, G., et al., *A potent cross-clade neutralizing human monoclonal antibody against a novel epitope on gp41 of human immunodeficiency virus type 1.* AIDS Res Hum Retroviruses, 2001. **17**(18): p. 1757-65.
11. Huang, J., et al., *Broad and potent neutralization of HIV-1 by a gp41-specific human antibody.* Nature, 2012. **491**(7424): p. 406.
12. Williams, L.D., et al., *Potent and broad HIV-neutralizing antibodies in memory B cells and plasma.* Science immunology, 2017. **2**(7).
13. Wild, C.T., et al., *Peptides corresponding to a predictive alpha-helical domain of human immunodeficiency virus type 1 gp41 are potent inhibitors of virus infection.* Proc Natl Acad Sci U S A, 1994. **91**(21): p. 9770-4.
14. Giannecchini, S., et al., *Antiviral activity and conformational features of an octapeptide derived from the membrane-proximal ectodomain of the feline immunodeficiency virus transmembrane glycoprotein.* J Virol, 2003. **77**(6): p. 3724-33.
15. Jiang, S., et al., *Inhibition of HIV-1 infection by a fusion domain binding peptide from the HIV-1 envelope glycoprotein GP41.* Biochem Biophys Res Commun, 1993. **195**(2): p. 533-8.
16. Jin, B.S., et al., *Design of a peptide inhibitor that blocks the cell fusion mediated by glycoprotein 41 of human immunodeficiency virus type 1.* AIDS Res Hum Retroviruses, 2000. **16**(17): p. 1797-804.
17. Kilby, J.M. and J.J. Eron, *Novel therapies based on mechanisms of HIV-1 cell entry.* N Engl J Med, 2003. **348**(22): p. 2228-38.
18. Wild, C.T., et al., *Peptides corresponding to a predictive alpha-helical domain of human immunodeficiency virus type 1 gp41 are potent inhibitors of virus infection.* 1994. **91**(21): p. 9770-9774.
19. Placone, J. and K. Hristova, *Direct assessment of the effect of the Gly380Arg achondroplasia mutation on FGFR3 dimerization using quantitative imaging FRET.* PLoS One, 2012. **7**(10): p. e46678.
20. Massi, C., et al., *The antiviral activity of a synthetic peptide derived from the envelope SU glycoprotein of feline immunodeficiency virus maps in correspondence of an amphipathic helical segment.* Biochemical and biophysical research communications, 1998. **246**(1): p. 160-165.
21. D'Ursi, A.M., et al., *Retroinverso analogue of the antiviral octapeptide C8 inhibits feline immunodeficiency virus in serum.* 2003. **46**(10): p. 1807-1810.
22. Scrima, M., et al., *Structural features of the C8 antiviral peptide in a membrane-mimicking environment.* Biochimica et Biophysica Acta (BBA)-Biomembranes, 2014. **1838**(3): p. 1010-1018.
23. Giannecchini, S., et al., *Feline immunodeficiency virus plasma load reduction by a retroinverso octapeptide reproducing the Trp-rich motif of the transmembrane glycoprotein.* Antivir Ther, 2005.

10(5): p. 671-80.

24. Del Piccolo, N., et al., *Production of plasma membrane vesicles with chloride salts and their utility as a cell membrane mimetic for biophysical characterization of membrane protein interactions.* Analytical chemistry, 2012. **84**(20): p. 8650-8655.

25. Baumgart, T., et al., *Large-scale fluid/fluid phase separation of proteins and lipids in giant plasma membrane vesicles.* Proc Natl Acad Sci U S A, 2007. **104**(9): p. 3165-70.

26. Grimaldi, M., et al., *Structural basis of antiviral activity of peptides from MPER of FIV gp36.* PLoS One, 2018. **13**(9): p. e0204042.

27. Di Marino, D., et al., *Binding of the Anti-FIV Peptide C8 to Differently Charged Membrane Models: From First Docking to Membrane Tubulation.* Front Chem, 2020. **8**: p. 493.

28. Merlino, A., et al., *Destabilization of lipid membranes by a peptide derived from glycoprotein gp36 of feline immunodeficiency virus: a combined molecular dynamics/experimental study.* 2012. **116**(1): p. 401-412.

29. Scott, R.E., *Plasma membrane vesiculation: a new technique for isolation of plasma membranes.* Science, 1976. **194**(4266): p. 743-745.

30. Levental, I., M. Grzybek, and K. Simons, *Raft domains of variable properties and compositions in plasma membrane vesicles.* Proceedings of the National Academy of Sciences, 2011. **108**(28): p. 11411-11416.

31. Veatch, S.L., et al., *Critical fluctuations in plasma membrane vesicles.* ACS chemical biology, 2008. **3**(5): p. 287-293.

32. Chen, L., et al., *Measuring the energetics of membrane protein dimerization in mammalian membranes.* Journal of the American Chemical Society, 2010. **132**(10): p. 3628-3635.

33. Del Piccolo, N., J. Placone, and K. Hristova, *Effect of thanatophoric dysplasia type I mutations on FGFR3 dimerization.* Biophysical journal, 2015. **108**(2): p. 272-278.

34. Scrima, M., et al., *Structural features of the C8 antiviral peptide in a membrane-mimicking environment.* Biochim Biophys Acta, 2014. **1838**(3): p. 1010-8.

2. *C8 properties on Tissue engineering and Differentiation on neuronal stem cells targets*

2.1 Introduction

As already mentioned in the first chapter, C8 is a peptide with eight residues (WEDWVGWI) belonging to the Membrane Proximal External Region (MPER) (**Figure 1**) of the mantle glycoprotein gp36 of FIV. It contains three evenly distributed Trp residues and exerts antiviral activity by inhibiting FIV entry into the host cell membrane.[1-7]

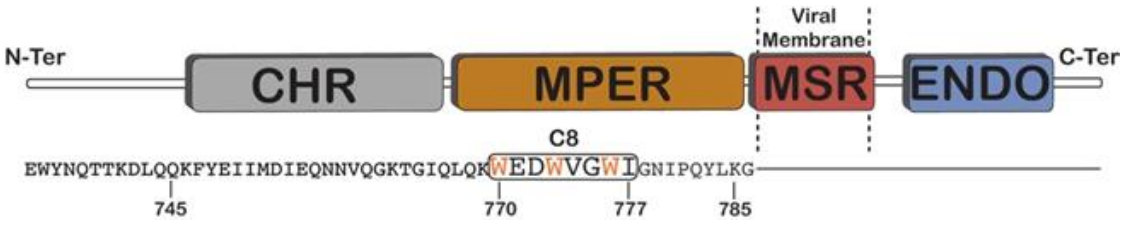

Figure 1. Graphic depiction of the C-terminal domains of the feline immunodeficiency virus (FIV) surface glycoprotein gp36-CHR-MPER. The black box displays the C8 peptide sequence, whereas the three tryptophans are highlighted in orange.

We have earlier produced spectroscopic data demonstrating that C8 is able of altering the lipid bilayers in various membrane-like systems [3, 7-12]

We examined the biophysical behavior of C8 using multiple membrane models to thoroughly identify the molecular mechanism regulating the interaction of C8 with the cell membrane.

Spectroscopy and molecular dynamics data showed that C8 interacts with the lipid interface, causing the entire membrane to be perturbed with increased lipid ordering and reduced dynamics. In particular, the adsorption of C8 strongly stiffens the outer region of the bilayer,

causing an effect that could be the first stage for a membrane rearrangement and remodeling, determining [13] the formation of membrane "nipples" and tubes to form a tight network of membrane connections. (**Figure 2**).[14, 15]

The ability of C8 to induce membrane tubulation was demonstrated even on vesicles[16, 17] derived from the native *Hela* cellular membrane.[16, 18, 19] In confocal microscopy imaging, we observed that C8 enhances vesicles movement, first to form vesicle collars and then to approach and merge in thin straight-chain tubular structures.

Tubule formation is a phase of membrane remodeling that is important for cell transport and communication.[20, 21] Membrane tubulation occurs in cell differentiation and the biological mechanism that drives tissue regeneration.[22] On this basis, a part of my Ph.D. research activity was focused on experiments aimed to test the ability of C8 to favor tissue regeneration. Specifically, 3D additively manufactured scaffolds with tailored morphology were developed and surface-modified using C8 peptide. Neat and peptide surface modified scaffolds were adequately analyzed. The biological features were evaluate of the 3D scaffolds to make adhesion of human neural stem cells (SH-SY5Y) and subsequently promote neuronal proliferation and differentiation.

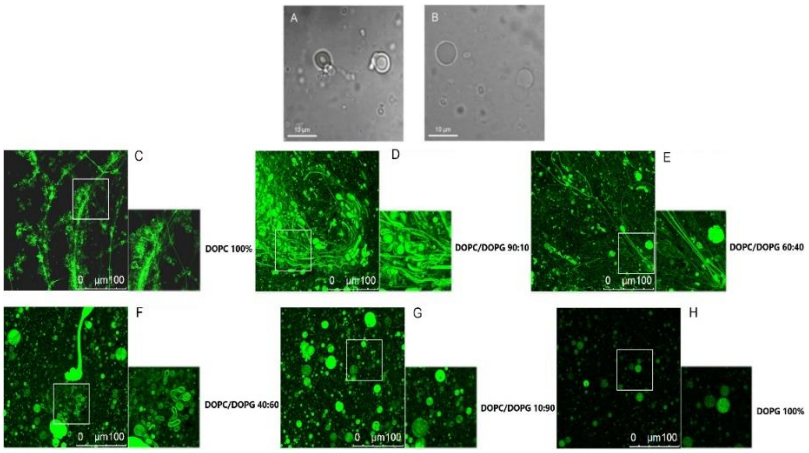

Figure 2. A-B Confocal microscopy imaging of MLVs in the absence of NBD labelled-C8 peptide. In A and B MLVs are composed of DOPC/DOPG 90:10 and 0:100 M/M, respectively. C-H: confocal microscopy imaging of MLVs in the presence of (NBD)-labelled-C8 peptide. MLVs vary in DOPC/DOPG composition as reported in the labels.[22]

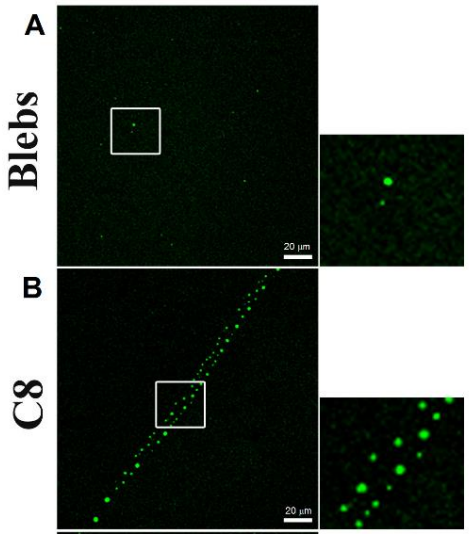

Figure 3. A) Blebs in the absence of labeled peptides. B) Confocal microscopy imaging of blebs in the presence of 0.5mM NBD labelled-C8 peptide.

2.2. Tissue engineering

Nowadays, neurological disorders are continuously growing with an ever-increasing aging population worldwide, resulting in 12% of global deaths [23]. Neurodegenerative diseases such as Alzheimer's and Parkinson's are destructive because neurons cannot be replaced in the diseased areas of the brain. Unfortunately, clinical treatments can hardly cure but only slow down the disease's progress.[24] Therefore, neurogenesis is under intense investigation [25] to improve neurodegenerative disease management. Indeed, the generation of new neurons from stem cells is considered for the potential to become a viable treatment option for patients suffering from neurodegenerative diseases.[26, 27]

The design of a scaffold in tissue engineering can guide the process of tissue regeneration, which is now one of the most challenging goals.[28] Cell adhesion to the scaffold surface is a critical factor in tissue engineering since adhesion occurs before other biological events such as cell spreading, migration, and differentiation.[29, 30] Polycaprolactone (PCL) is a well-known and commercially available polymer with promising potential in biomedical applications.[31] It is biocompatible and biodegradable and therefore widely investigated to

develop scaffolds for tissue regeneration to improve delivery systems and implants. Its biodegradability depends on its vulnerability to hydrolysis of its ester linkage: the generated products are non-toxic and can either be metabolized via the tricarboxylic acid cycle or eliminated by direct secretion.[32]

2.3 Results

2.3.1 Peptide Synthesis

C8 peptide was synthesized by the Fmoc solid-phase synthesis method according to the previously published procedure.[12] For the confocal microscopy analysis, the C8 peptide was synthesized to include Dap (l-diamino propionic acid) amino acid in substitution of 770W according to the solid phase synthesis methods using Fmoc-Dap(NBD)-OH. This was obtained by alkylating the free amino group of Nα-Fmoc, l-diamino propionic acid (Fmoc-Dap-OH) with NBD chloride.[13]

2.3.2 3D-PLC Scaffold bio- functionalization

The procedure of 3D-PLC Scaffold bio- functionalization included the following steps:

1. Aminolysis of 3D PCL Scaffolds: First 1, 6-hexanediamine (DEA) was linked to the surface of 3D PCL. Briefly, 3D fiber-deposited scaffolds were immersed at different times in 0.08 g/mL DEA/isopropanol (IPA) solution at 37 °C. Then, the aminolysis reaction was carried out in a custom-made reactor thermostat in a water bath with adequate magnetic stirring for a suitable time. After the aminolysis treatment, the scaffolds were rinsed with deionized water at room temperature for 24 h. Successively, they were dried in a vacuum desiccator and stored at room temperature.
2. Determination of Engrafted Amines: A ninhydrin-based procedure (Kaiser Test, Aldrich) was employed to assess the presence of amino groups on the PCL-NH2 scaffolds.

3. Peptide Conjugation: C8 peptide was covalently grafted onto the surface in a two-step way by using an epoxy cross-linker in mild aqueous conditions. First, the aminolyzed 3D scaffolds were treated with a 5% diethylene glycol diglycidyl ether (DGDGE) in a sodium carbonate solution (50 mM, pH 8.5) at room temperature, gently shaking for 3 h. Subsequently, the ether solution was rinsed out, and the scaffolds were washed thoroughly with water. The conjugation step was performed adding 0.2 mg/mL of C8 peptide in sodium carbonate solution (50 mM, pH = 8.5). For the determination of peptide conjugation, Kaiser Test was performed. An ethanolamine (2 mM) aqueous solution was used to deactivate unreacted groups. A scheme of the two-step procedure employed to graft C8 peptide on PCL fibers of the 3D scaffolds is reported in **Figure 4**.

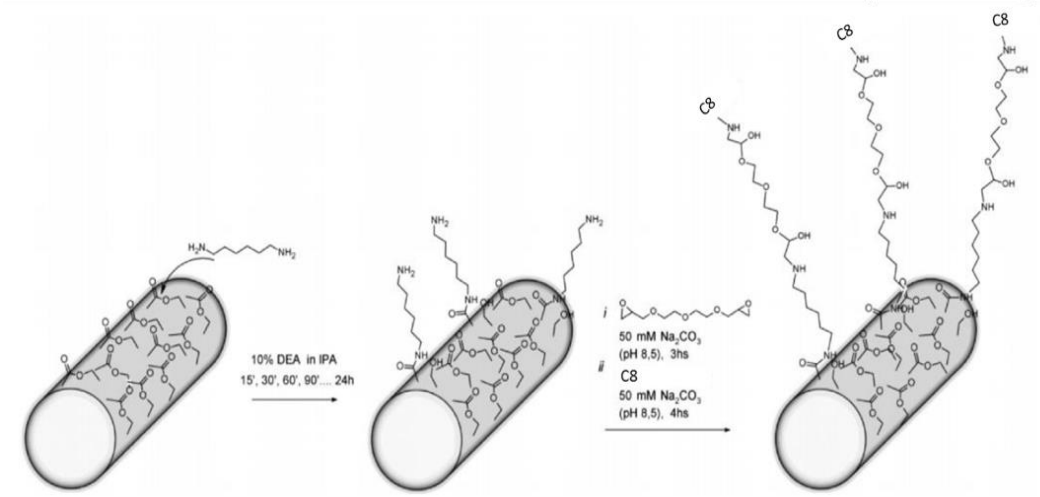

Figure 4. Scheme of the two-step procedure used to graft C8 peptides to PCL fibers of the 3D scaffolds. DEA and IPA indicate 1, 6-hexanediamine and isopropanol, respectively. The chemical structure of C8 is also reported.

2.3.3. Determination of Engrafted Amines and Conjugated Peptide

Following aminolysis, an analytical assessment of amino groups engrafted onto the surface of PCL fibers composing the additively manufactured 3D scaffold was carried out using a slightly modified Kaiser test technique.[30, 33, 34] The results were consistent with those reported in previous work.[28]

2.3.4 Mechanical characterization

Tensile tests showed a ductile behavior for both neat PCL fibers and peptide surface-modified PCL fibers. In particular, the obtained stress−strain curves showed an initial linear region, then a slight decrease in the slope occurred up to a local maximum stress value, followed by a decrease of the tensile stress. Successively, a plateau-like region was evident, and finally, a new increase of stress was observed until failure was generally reached.

During testing, the propagation of multiple necks was also observed along the peptide surface-modified PCL fibers in comparison with the neat ones, as evidenced by the fluctuating stress values after the first local maximum of the curve. Such results are consistent with those previously reported in the literature.

Furthermore, even though the two-step surface treatment strongly reduced the maximum strain, it did not alter modulus (E) and yield stress (σ_y).

Table 1. Results from tensile tests performed on neat and peptide surface-modified PCL: tensile modulus (E), yield stress (σ_y), and maximum strain (ε_{max}). The results are reported as mean value ± standard deviation.

	E (MPa)	**σ_y (MPa)**	**ε_{max} (mm/mm)**
Neat Fibers	548.3 ± 55.3	24.4 ± 2.1	12.3 ± 1.2
Peptide Surface Modified Fibers	533.2 ± 58.4	23.8 ± 2.5	6.8 ± 0.8

Results from compression tests evidenced the influence of the two-step surface treatment on the mechanical behavior of the PCL scaffolds.

The stress-strain curves (**Figure 5**) obtained for neat and peptide surface-modified scaffolds were consistent with those reported for 3D printed PCL structures.

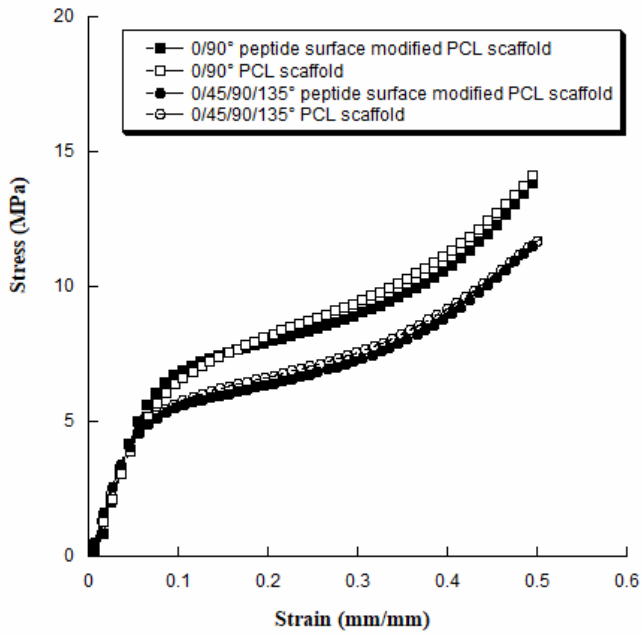

Figure 5. Typical stress-strain curves obtained from compression tests on neat and peptide surface modified PCL scaffolds with 0/90° and 0/45/90/135° lay-down pattern (rate of 1 mm/min, final strain of 50%).

Table 2. Compressive modulus and maximum stress for PCL scaffolds characterized by different lay-down patterns (i.e. 0/90° and 0/45/90/135°), before and after the two-step surface modification. The results are reported as mean value ± standard deviation.

	Neat Scaffolds		**Peptide Surface Modified Scaffolds**	
Pattern	**E (MPa)**	**σ (MPa)**	**E (MPa)**	**σ (MPa)**
0/90°	90.2 ± 7.1	14.3 ± 1.1	89.8 ± 9.1	14.1 ± 1.2
0/45/90/135°	70.1 ± 6.2	11.8 ± 1.0	68.4 ± 7.5	11.6 ± 1.1

Values of compressive modulus and maximum stress are reported in **Table 2**. The lay-down pattern influenced the mechanical behavior of the additive manufactured PCL scaffolds. In particular, scaffolds with a 0/90° pattern showed compressive modulus and maximum stress values, which are significantly greater than those found in the 0/45/90/135° pattern. These findings are consistent with those reported in the literature.

Furthermore, it is worth noting that the two-step treatment did not significantly alter the micromechanical behavior of the additive manufactured scaffolds. No statistically significant differences were found in terms of compressive modulus and maximum stress before and after the two-step treatment (**Table 2**).

Nanoindentation tests were carried out on aminolyzed and not-aminolyzed PCL fibers. These were characterized by a diameter (D) of 340−360 μm and obtained through a Bioplotter dispensing machine (Envisiontec GmbH, Germany). All nanoindentation measurements on PCL fibers highlighted differences in load-depth curves and hence, hardness values. Both peptide surface modified and neat PCL fibers evidenced hardness (H) values that generally decrease as load increases from 1 to 5 mN. Specifically, hardness values ranged from 0.54 ± 0.02 GPa to 0.29 ± 0.01 GPa and from 0.13 ± 0.02 GPa to 0.05 ± 0.01 GPa for neat PCL fibers and peptide surface-modified fibers, respectively, in the load range investigated (**Figure 6**).

The final results suggested that the fiber surface became softer after the two-step treatment.

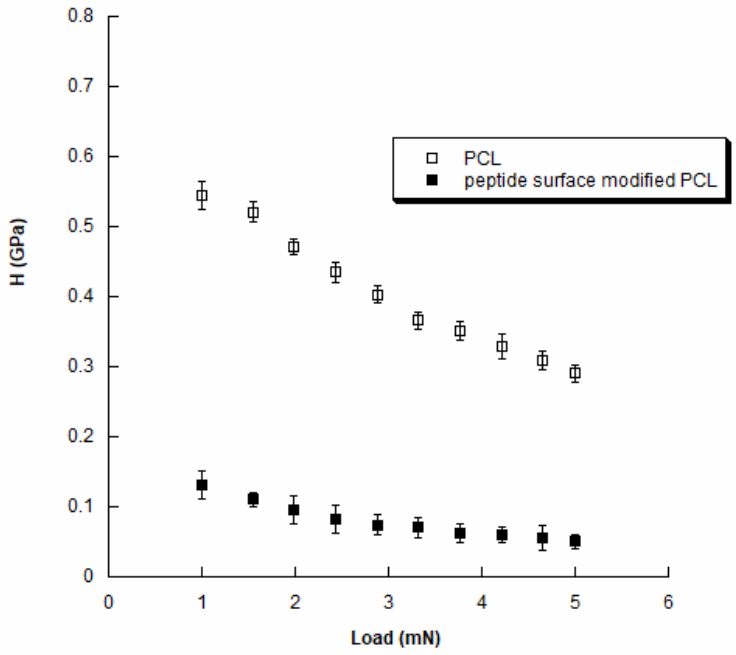

Figure 6. Results obtained from nanoindentation tests on neat and peptide surface-modified fibers: hardness as a function of the applied load (1−5 mN). Data are graphically reported as mean value, and bars represent the standard deviation.

2.3.5. Biological Analysis

- **Preliminary biological assessment**

In order to evaluate the effect of C8 peptide on cell adhesion and proliferation, preliminary biological analyses were performed. In particular, to assess the effect of C8 peptide on cell adhesion and proliferation, SHSY5Y cells on gelatinized well-plates, SHSY5Y cells with 5 μM retinoic acid in DMEM, SHSY5Ycells with 22 μM C8 peptide in DMEM were considered.

At 3 days from seeding, cell adhesion on gel-coated well-plates was confirmed by Alamar Blue assay (data not shown).

Cell morphology was analyzed using Confocal Laser Scanning Microscopy (CLSM). **Figure 7** reports the results of CLSM analyses performed on SHSY5Y cells on gelatinized well-plates, containing 5 μM retinoic acid in DMEM, and 22 μM C8 peptide, respectively. Confocal microscopy imaging was acquired in DMEM at 3 days from seeding. β-III tubulin staining was used to observe SHSY5Y, C8 - SHSY5Y cells, and RA – SHSY5Y; DAPI staining was used for SHSY5Y, c8 - SHSY5Y cells, and RA – SHSY5Y cells. Analysis of the data indicates that β-III tubulin expression was qualitatively higher when SHSY5Y cells were treated with C8 peptide compared to the other samples (**Figure 7**). Furthermore, SHSY5Y cells appeared more elongated when treated with C8 peptide, suggesting they tended to differentiate probably promoting neuronal formation.

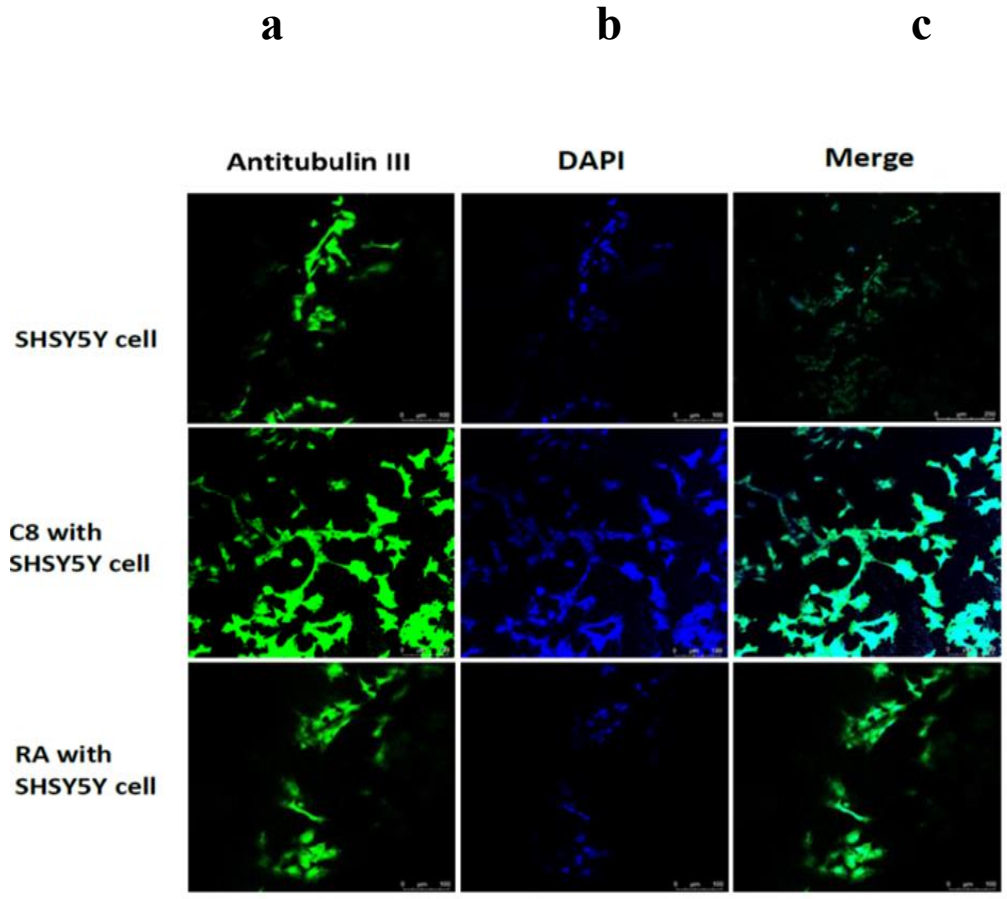

Figure 7: CLSM analyses performed on SHSY5Y cells on gelatinized well-plates, SHSY5Y cells with 5 µM retinoic acid in DMEM, SHSY5Y cells with 22 µM C8 peptide in DMEM at 3 days from seeding. **a**: β-III tubulin staining for SHSY5Y, C8 - SHSY5Y cells and RA – SHSY5Y. **b**: DAPI statining for SHSY5Y, c8 - SHSY5Y cells and RA – SHSY5Y cells. **c**: Merge.

- **Biological analyses on 3D cell constructs**

To deepen the study on the effect of C8 on tissue regeneration, C8 functionalized 3D scaffolds were prepared by following the previously reported procedure, and the ability to affect cell regeneration was observed as before.

8 x 10^4 cells were seeded on peptide surface-modified 3D scaffolds, according to the test method described in "2.4.6. Biological Analysis" section. PCL 3D scaffolds were selected as control.

Cell viability/proliferation was evaluated by Alamar Blue assay at different time points. Data

are reported as mean ± standard deviation, and values of %reduction of Alamar Blue assay over time were normalized and reported as cell density over time.

One hundred microliters of the solution were subsequently removed from the wells and transferred to a new 96-well plate. The optical density was immediately measured with a spectrophotometer at 540 and 600 nm wavelengths. According to the manufacturer's protocol, the number of viable cells correlates with the magnitude of dye reduction and is expressed as a percentage of Alamar Blue reduction. **Figure 8** reports the results obtained from the Alamar Blue assay. A general increase of Alamar Blue **%**reduction over time indicates that cells could survive and proliferate throughout the scaffolds.

Furthermore, cell morphology was also analysed through Confocal Laser Scanning Microscopy (CLSM). CLSM analyses highlighted that SH-SY5Y cells were already able to adhere on the PCL fiber of the 3D scaffolds, also showing a morphology that drastically changes on the different samples over time (**Figure 9**).

In particular, regarding neat PCL scaffolds, cells appear more rounded, indicating a scarcer adhesion to the substrate if compared to the results obtained for the peptide surface-modified PCL scaffolds. Thus, the two-step treatment led to better cell adhesion and spreading on the fiber surface, evidencing a good interaction with the material.

Furthermore, the effect of the two-step treatment on 3D PCL scaffolds was more visible at 7, 14, and 21 days after cell seeding (**Figure 9**). Specifically, as for cell morphology, in the case of peptide surface-modified scaffolds, better SH-SY5Y spreading was evident, highlighting a cell alignment in a specific direction. Such effect may be probably due to a synergic contribution of the surface chemistry and topography of the additive manufactured scaffolds.

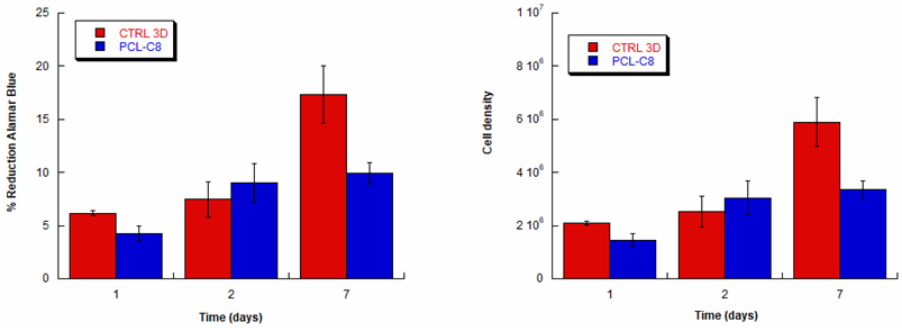

Figure 8. Alamar Blue assay performed on cell-scaffold constructs (neat and peptide surface-modified 3D scaffolds): results reported as a percentage of Alamar Blue reduction and cell density (mean value ± standard deviation) at 1, 2 and 7 days after cell seeding.

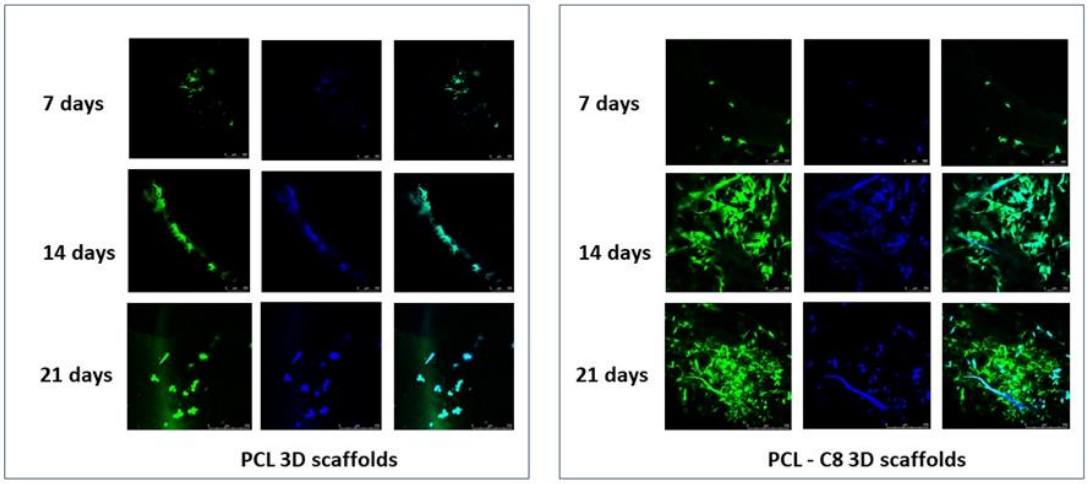

Figure 9. Typical results from CLSM analysis on neat and peptide surface modified scaffolds at 7, 14, and 21 days after cell seeding.

2.4 Conclusion

Starting from data previously acquired in our lab that C8 is capable of destabilizing cell membranes inducing the formation of membrane tubes, in the reported part of my Ph D activity we investigated the possibility that this property of C8 can be valuably used to promote cell differentiation and tissue regeneration.

Therefore we produced C8 functionalized PCL scaffolds and evaluated the ability of these devices to affect SH-SY5Y neuronal cells. Our data show that PCL can be efficiently functionalized with C8, and these scaffolds are efficient to promote cell proliferation with modification of their shapes.

In particular, CLSM analysis indicated that cells exhibit a scarcer adhesion on neat PCL scaffolds if compared to the cells on the peptide surface-modified PCL scaffolds. Thus, PCL C8 functionalization induces better cell adhesion and spreading on the fiber surface, evidencing the ability to improve interaction with the material.

Moreover, peptide surface-modified scaffolds induce better SH-SY5Y spreading, highlighting a cell alignment in a specific direction. Such effect may probably be due to a synergic contribution of the surface chemistry and topography of the additive manufactured scaffolds.

2.5 Materials and methods

2.5.1 Peptide synthesis

The C8 was synthesized by fluorenylmethyloxycarbonyl chloride (Fmoc) solid phase peptide synthesis (SPPS) methodology according to the previously published procedure.[35] C8 with sequence residue ^{770}WEDWVGWI^{777} (**Figure 10A**) and for the confocal microscopy analysis, all peptides labelled with nitrobenzoxadiazole (NBD) fluorophore and the L-diamino propionic acid Fmoc-Dap (NBD)-OH) [13] which were used in substitution of 770W.??????? Labelled C8 peptide was prepared by synthesizing Ac-^{770}Dap (NBD)EDWVGWI^{777}-NH2 (**Figure.10B**). Accordingly, the peptides were synthesized manually (100mg scale) in disposable 5mL polypropylene reactors fitted with a PTFE filter by using acidic resin (Wang) 200 mg (1.1 mmol/g). The resin was swelled in DMF for 2 h at room temperature. The resin was washed with DMF (2× 20s with 2 mL).

HBTU (2-(1H-benzotriazol-1-yl)-1,1,3,3-tetramethyluronium hexafluorophosphate,

Hexafluorophosphate Benzotriazole Tetramethyl Uronium), HOBT (Hydroxybenzotriazole) and N,N¢-diisopropylethylamine (DIEA) were a coupling reagent used in DMF as a solvent to solid phase synthesis. Deprotection of the Fmoc group was affected with 20% piperidine in DMF. Following synthesis, the peptide-resin was washed with DCM and dried in vacuo.

The resin was treated with cleavage cocktail (TFA/H2O/TIS (95: 2.5: 2.5, 3 mL)) for 2 h, filtered, and washed two time with the same cleavage cocktail (1mL). TFA was removed by evaporation and the product precipitated in ether. The product was washed with ether (3 · 2 mL), dried and lyophilized.

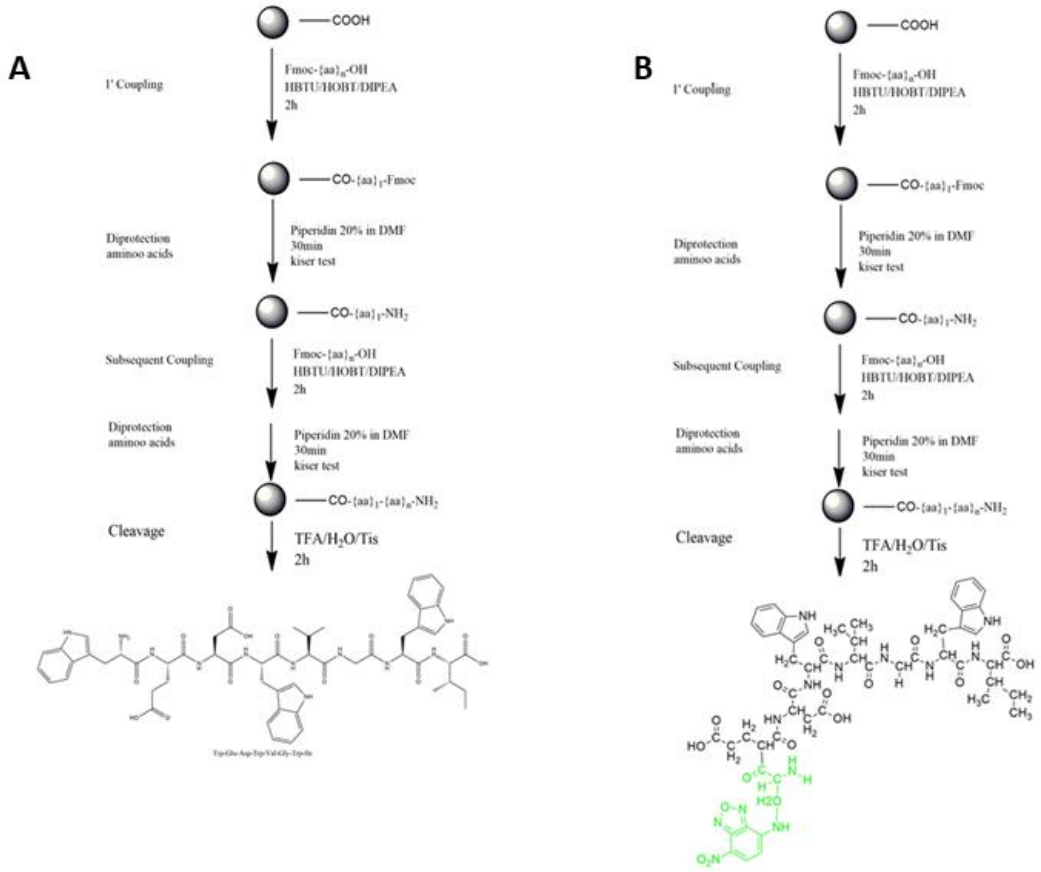

Figure 10 (A) C8 and (B) C8 labelled peptide synthesis by solid phase synthesis protocols.

2.5.2 3D Scaffolds Design and Preparation

3D poly(ε-caprolactone) scaffolds were fabricated by additive manufacturing.

Specifically, poly(ε-caprolactone) (PCL, Mw = 65000; Sigma-Aldrich, St. Louis, MO)

pellets were processed through the 3D fiber deposition technique.

3D scaffolds were obtained by alternatively extruding and depositing the polymer fibers with different angle steps between two successive layers, making two different patterns: 0°/90° and 0°/45°/90°/135°.

The nozzle used to inject/extrude PCL fibers was a stainless steel needle characterized by an inner diameter of 400 μm. Each scaffold was characterized by the fiber diameter (depending on the needle diameter and/or the deposition speed), as well as by the fiber spacing (strand distance, i.e. center-to-center distance) and layer thickness, which influence the overall pore size. The values of strand distance and layer thickness were set to 640 μm and 320 μm.

2.5.3 Mechanical characterization

Tensile tests were performed on neat PCL fibers and peptide surface modified PCL fibers (340−360 μm in diameter - D), using an INSTRON 5566 testing and a gauge length of 20 mm. The tests were carried out according to the ASTM D3822 standard.

Compression tests were carried out on neat and peptide surface modified 3D scaffolds using block-shaped specimens (length—L_0 of 7.0 mm, width—W_0 of 7.0 mm, height—H_0 of 7.8 mm). The specimens were compressed to a strain of 50% at a rate of 1 mm/min, using an INSTRON 5566 testing machine. Taking into account the measured force F and the initial cross-sectional area of the specimen ($A_0 = Lo \cdot W_0$), the "apparent" stress (σ) was calculated as $\sigma = F/A_0$. The strain (ε) was defined as the ratio between the scaffold height variation Δh and its initial height h_0 ($\varepsilon = \Delta h/h_0$).

Nanoindentation analyses were performed using the Nano test Platform (Micromaterials, U.K.) in a specific load range (1–5 mN). A diamond pyramid-shaped Berkovich-type indenter tip was employed. The trapezoidal load functions characterised by the specific values for the load hold periods (i.e., 20 s) and the loading–unloading rates (i.e., 300 μN/s) were considered. Using the Oliver and Pharr method[36], the hardness values were evaluated from the load-depth

curves.

Hardness (H) was evaluated considering the applied peak load (P_{max}) and the projected contact area (Ac) at the specified load, according to the equation $H = P_{max}/A_c$. The projected contact area A_c is strongly related to the geometry of the indenter, and it can be calculated from the penetration depth.

2.5.4 Aminolysis of 3D PCL Scaffolds

This procedure, which was already shown in a previous work [30] was used to insert covalently amino groups onto the fiber surface of the 3D PCL scaffolds, using 1,6-hexanediamine (DEA). Briefly, 3D fiber-deposited scaffolds were immersed at different times in 0.08 g/mL DEA/isopropanol (IPA) solution at 37 °C. The aminolysis reaction was carried out in a custom-made reactor thermostat in a water bath with adequate magnetic stirring for a suitable time, in batch mixer processing conditions. After the aminolysis treatment, solution was removed, and the scaffolds were rinsed with deionized water at room temperature for 24 h. Successively, they were dried in a vacuum desiccator and stored at room temperature for further modifications.

2.5.5 Determination of Engrafted Amines

In order to assess the number of amino groups on the PCL-NH_2 scaffolds a ninhydrin-based procedure (Kaiser test, Aldrich) was employed. The samples were dissolved in kit solutions and heated at 100 °C for 15 min. Afterward, at room temperature methylene chloride/ethanol solution was added to stabilize the blue compound and to bring the polymer mixture into solution. The absorbance was measured at 570 nm using an UV−vis spectrophotometer (Lambda 25, Perkin-Elmer).

A calibration curve was obtained by 1,6-hexaneamine in methylene chloride/ethanol solution. Each experiment was performed at least three times in triplicate.

2.5.6 Biological Analysis

Preliminary biological assessment

In order to evaluate the effect of C8 peptide on cell adhesion and proliferation, preliminary biological analyses have been performed. Briefly, SH-SY5Y Cell Line human Neuroblast from neural tissue was used. SH-SY5Y cells were maintained at 37°C and 5% CO_2 in Dulbecco's modified Eagle medium (DMEM, high glucose) supplemented with 10% fetal bovine serum (FBS, BioWhittaker, Walkersville, MD), 2 mM L-glutamine (Sigma, St. Louis, MO), 1000 U/l penicillin (Sigma, St. Louis, MO) and 100 mg/l streptomycin (Sigma, St. Louis, MO).

After the incubation time, 8 x 10^4 cells were seeded on gelatin-coated 6 well plates (gelatin 1% by weight) and grown in enriched DMEM-w/o FBS to avoid unspecific cell adhesion depending on serum protein adsorption.

In particular, in order to evaluate the effect of C8 peptide on cell adhesion and proliferation, SHSY5Y cells on gelatinized well-plates, SHSY5Y cells with 5 μM retinoic acid in DMEM, SHSY5Y cells with 22 μM C8 peptide in DMEM were considered.

At 3 days from seeding, cell adhesion on gel-coated well-plates were investigated by Alamar Blue assay (data not shown).

Cell morphology was also analysed using Confocal Laser Scanning Microscopy (CLSM). Firstly, cells were fixed with 4% paraformaldeyde for 20 min at room temperature, permalized in 0.5% Triton-X100 and 1% BSA in PBS for 10 minutes. Cells were rinsed twice with PBS and incubated with PBS-BSA 0.5% to block unspecific binding.

After washing step with PBS for 5 minutes, cells were incubated with anti-tubulin III primary antibody diluted in blocking solution for 2h at room temperature. Samples were rinsed in PBS. For the binding of secondary antibody, Goat Antirabbit IgG FITC conjugated was incubated for 1 h at room temperature before washing samples 3 times for 10 minutes in PBS. Moreover, cells nuclei were stained with DAPI (300 ng/ml in PBS). The images were acquired at 3 days from seeding.

Biological analyses on 3D cell constructs

SH-SY5Y Cell Line human Neuroblast from neural tissue was used. SH-SY5Y cells were maintained at 37°C and 5% CO_2 in Dulbecco's modified Eagle medium (DMEM, high glucose) supplemented with 10% fetal bovine serum (FBS, BioWhittaker, Walkersville, MD), 2 mM L-glutamine (Sigma, St. Louis, MO), 1000 U/l penicillin (Sigma, St. Louis, MO) and 100 mg/l streptomycin (Sigma, St. Louis, MO).

After the incubation time, 8 x 10^4 cells were seeded on 3D scaffolds surface modified with C8 peptide. Cell viability/proliferation was evaluated by Alamar Blue assay at different time points. Data are reported as mean ± standard deviation and values of %reduction of Alamar Blue assay over time were normalized and reported also as cell density over time.

One hundred microliters of the solution were subsequently removed from the wells and transferred to a new 96-well plate. The optical density was immediately measured with a spectrophotometer at wavelengths of 540 and 600 nm. The number of viable cells correlates with the magnitude of dye reduction and is expressed as a percentage of Alamar Blue reduction, according to the manufacturer's protocol.

Alamar Blue assay is based on a redox reaction that occurs in the mitochondria of the cells; the colored product is transported out of the cell and can be measured spectrophotometrically. After 3 days of incubation, the cells were rinsed with PBS (Sigma-Aldrich, Italy), and for each sample, 200 µl of Dulbecco's modified Eagle's medium (DMEM) without Phenol Red (HyClone, UK) containing 10% (v/v) Alamar Blue (AbD Serotec Ltd, UK) was added, followed by incubation in 5% CO_2 diluted atmosphere for 4 hours at 37°C.

Cell morphology was also analysed through Confocal Laser Scanning Microscopy (CLSM). Firstly, cells were fixed with 4% paraformaldeyde for 20 min at room temperature, permalized in 0.5% Triton-X100 and 1% BSA in PBS for 10 minutes. Cells were rinsed twice with PBS and incubated with PBS-BSA 0.5% to block unspecific binding. After washing step with PBS for 5 minutes, cells were incubated with anti-enolase primary antibody diluted in blocking

solution for 2h at room temperature. Samples were rinsed in PBS. For the binding of secondary antibody, Goat Antirabbit IgG FITC conjugated was incubated for 1 h at room temperature before washing samples 3 times for 10 minutes in PBS. Moreover, cells nuclei were stained with DAPI (300 ng/ml in PBS). The images were acquired at 7, 14 and 21 days from seeding.

2.6 References

1. Grimaldi, M., et al., NMR structure of the FIV gp36 C-terminal heptad repeat and membrane-proximal external region. 2020. **21**(6): p. 2037.
2. Lombardi, S., et al., Inhibition of feline immunodeficiency virus infection in vitro by envelope glycoprotein synthetic peptides. Virology, 1996. **220**(2): p. 274-84.
3. Giannecchini, S., et al., Antiviral activity and conformational features of an octapeptide derived from the membrane-proximal ectodomain of the feline immunodeficiency virus transmembrane glycoprotein. J Virol, 2003. **77**(6): p. 3724-33.
4. Pancino, G., et al., Structure and variations of feline immunodeficiency virus envelope glycoproteins. Virology, 1993. **192**(2): p. 659-62.
5. Wyatt, R. and J. Sodroski, The HIV-1 envelope glycoproteins: fusogens, antigens, and immunogens. Science, 1998. **280**(5371): p. 1884-8.
6. Eckert, D.M., et al., Inhibiting HIV-1 entry: discovery of D-peptide inhibitors that target the gp41 coiled-coil pocket. Cell, 1999. **99**(1): p. 103-15.
7. Frey, S.C., E.A. Hoover, and J.I. Mullins, Feline immunodeficiency virus cell entry. J Virol, 2001. **75**(11): p. 5433-40.
8. Di Marino, D., et al., Binding of the Anti-FIV Peptide C8 to Differently Charged Membrane Models: From First Docking to Membrane Tubulation. Front Chem, 2020. **8**: p. 493.
9. Chan, D.C., et al., Core structure of gp41 from the HIV envelope glycoprotein. Cell, 1997. **89**(2): p. 263-73.
10. Whitmore, L. and B.A. Wallace, The Peptaibol Database: a database for sequences and structures of naturally occurring peptaibols. Nucleic Acids Res, 2004. **32**(Database issue): p. D593-4.
11. Lamb, R.A. and T.S. Jardetzky, Structural basis of viral invasion: lessons from paramyxovirus F. Curr Opin Struct Biol, 2007. **17**(4): p. 427-36.
12. Serres, P.F., Molecular mimicry between the trimeric ectodomain of the transmembrane protein of immunosuppressive lentiviruses (HIV-SIV-FIV) and interleukin 2. C R Acad Sci III, 2000. **323**(11): p. 1019-29.
13. Dufau, I. and H. Mazarguil, Design of a fluorescent amino acid derivative usable in peptide synthesis. Tetrahedron Letters, 2000. **41**(32): p. 6063-6066.
14. Amodio, G., et al., Identification of a microRNA (miR-663a) induced by ER stress and its target gene PLOD3 by a combined microRNome and proteome approach. Cell biology and toxicology, 2016. **32**(4): p. 285-303.
15. Amodio, G., et al., Endoplasmic reticulum stress reduces COPII vesicle formation and modifies Sec23a cycling at ERESs. FEBS letters, 2013. **587**(19): p. 3261-3266.
16. Montagnier, L., 25 years after HIV discovery: prospects for cure and vaccine. Virology, 2010. **397**(2): p. 248-54.
17. Lee, T., et al., Analysis of the S3 and S3 ' subsite specificities of feline immunodeficiency virus (FIV) protease: Development of a broad-based protease inhibitor efficacious against FIV, SIV and HIV in vitro and ex vivo. Proceedings of the National Academy of Sciences of the United States of America, 1998. **95**(3): p. 939-944.
18. Bendinelli, M., et al., Feline immunodeficiency virus: an interesting model for AIDS studies and an important cat pathogen. Clin Microbiol Rev, 1995. **8**(1): p. 87-112.
19. Dunham, S.P., Lessons from the cat: development of vaccines against lentiviruses. Vet Immunol Immunopathol, 2006. **112**(1-2): p. 67-77.
20. Yue, T., X. Zhang, and F. Huang, Molecular modeling of membrane tube pearling and the effect of nanoparticle adsorption. Phys Chem Chem Phys, 2014. **16**(22): p. 10799-809.
21. Ariga, K., et al., Challenges and breakthroughs in recent research on self-assembly. Sci Technol Adv Mater, 2008. **9**(1): p. 014109.
22. Grimaldi, M., et al., Structural basis of antiviral activity of peptides from MPER of FIV gp36. PLoS One, 2018. **13**(9): p. e0204042.
23. Samaridou, E., et al., Nose-to-brain delivery of enveloped RNA - cell permeating peptide nanocomplexes for the treatment of neurodegenerative diseases. Biomaterials, 2020. **230**: p. 119657.
24. Niu, X., J. Chen, and J. Gao, Nanocarriers as a powerful vehicle to overcome blood-brain barrier in treating neurodegenerative diseases: Focus on recent advances. Asian J Pharm Sci, 2019. **14**(5): p. 480-496.
25. Gorman, A.M., Neuronal cell death in neurodegenerative diseases: recurring themes around protein handling. J Cell Mol Med, 2008. **12**(6a): p. 2263-80.
26. Kim, S.U., H.J. Lee, and Y.B. Kim, Neural stem cell-based treatment for neurodegenerative diseases.

Neuropathology, 2013. **33**(5): p. 491-504.
27. Kang, J.M., et al., Stem Cell Therapy for Alzheimer's Disease: A Review of Recent Clinical Trials. J Alzheimers Dis, 2016. **54**(3): p. 879-889.
28. Gloria, A., et al., Three-dimensional poly(ε-caprolactone) bioactive scaffolds with controlled structural and surface properties. Biomacromolecules, 2012. **13**(11): p. 3510-21.
29. Ko, Y.G., et al., Immobilization of poly(ethylene glycol) or its sulfonate onto polymer surfaces by ozone oxidation. Biomaterials, 2001. **22**(15): p. 2115-23.
30. Causa, F., et al., Surface investigation on biomimetic materials to control cell adhesion: the case of RGD conjugation on PCL. Langmuir, 2010. **26**(12): p. 9875-84.
31. Ashammakhi, N., et al., Tissue engineering: a new take-off using nanofiber-based scaffolds. J Craniofac Surg, 2007. **18**(1): p. 3-17.
32. Harmankaya, N.J.D.B.s.t., Enhanced endothelialisation of electrospun poly (caprolacetone) with pegylated cell-adhesive peptide sequences: Potential use in tissue engineered vascular scaffolds. 2007.
33. Kaiser, E., et al., Color test for detection of free terminal amino groups in the solid-phase synthesis of peptides. Anal Biochem, 1970. **34**(2): p. 595-8.
34. Sarin, V.K., et al., Quantitative monitoring of solid-phase peptide synthesis by the ninhydrin reaction. Anal Biochem, 1981. **117**(1): p. 147-57.
35. Scrima, M., et al., Structural features of the C8 antiviral peptide in a membrane-mimicking environment. Biochim Biophys Acta, 2014. **1838**(3): p. 1010-8.
36. Pharr, G. and W.J.M.B. Oliver, Measurement of thin film mechanical properties using nanoindentation. 1992. **17**(7): p. 28-33.

3. *Conformational analysis of peptide derived from Gp36 NHR region.*

3.1 Introduction

FIV's gp36 and HIV's gp41 induce virus envelope fusion with the host cell membranes. They both have a similar framework (**Figure 1**) [1-3] that includes the fusion peptide (FP), N-terminal heptad repeat (NHR), C-terminal heptad repeat (CHR), and membrane-proximal extracellular region (MPER). MPER is a hydrophobic, Trp-rich region (**Figure 1**) characterized by a strong membrane affinity. Virus entry is effective once NHR and CHR fold back to form a low-energy stable six-helical bundle (6HB);[4], MPER plays a significant role by correctly driving the virus to assemble with the host cell membrane.

Gp41 and Gp36 conformational rearrangement can be efficiently inhibited by peptides mimicking conserved functional elements in Gp41 or Gp36. A prominent example of such peptides, termed fusion inhibitors, is the peptide T-20 (enfuvirtide, Fuzeon), used as salvage therapy for HIV/AIDS.[5]

In a similar experimental approach, we previously identified C8, a peptide belonging to the Gp36 MPER that exhibited significant anti-FIV activity in vitro and in vivo.

Therefore, in an attempt to design anti-FIV analogous of C8, a strand of research carried out over the years in our laboratory has focused on the study of C8 concerning i) its mechanism of action, ii) its biophysical behavior on membranes of biological interest, iii) the study of an extended region of MPER corresponding to CHR-MPER, iv) the study of molecules belonging to Gp36 and potential interferents of C8 action.

The rational design of peptides capable of inhibiting the formation of 6HB in Gp36 takes significant advantage of structural information on the fragments that may interact with each

other. Specifically, it would be advantageous to understand how in the Gp36 six-helix bundle TM interacts with FP, NHR with CHR, and PR with MPER. This information can be obtained at different accuracy based on experimental or computational evidence. Robust structural data can be derived by NMR or crystallographic analysis. However, solving an NMR structure is dramatically time-consuming and implies high economic expenditure. On the other hand, structural information can be valuably extracted by computational procedures using different protocols of molecular simulation.

Moved from the antiviral activity of C8, unusual for a small peptide, we previously performed an extensive biophysical analysis to elucidate the molecular mechanism underlying its activity.[12, 13] C8, as part of MPER, exerts its activity at the interface between the host cell membrane and the PR region of Gp36. Deepening the exploration of C8 as part of MPER we studied in membrane mimicking micelle solution, the NMR structure of a construct including the full MPER, and part of the CH region. To identify peptides interacting with CH-MPER capable of destabilizing the Gp36 6HB, we focused on peptide sequences deriving from the NHR region. Interestingly, the peptide corresponding to the sequence 627-646 of Gp36 NHR (named C20) previously was found [14] to inhibit C8 activity. In the hypothesis that this activity may be based on a structural interaction between C20 and the region in gp36 includes C8, part of my Ph.D. activity focused on studying C20 NMR structure as a preliminary step to characterize the interaction with CH-MPER.

NMR-based analysis of protein-ligand interactions, specifically protein-protein or peptide-protein interactions, can take advantage of the so-called “protein observed” and “ligand-observed” experiments.[6-8] The appropriate experimental procedure depends on the molecular size and, in particular, on the difference in the size of the two interacting molecules.

To study interaction of C20 with CH-MPER, the most appropriate approach consists of Protein-Observed Experiments that involve studying the three-dimensional structure of the protein target (in our case CHR-MPER). Once the structural models of the target protein are

known, the interaction between the two molecules is observed using Chemical Shift Mapping experiments.[9, 10] Accordingly, the change in the chemical shifts of the protein signals is monitored in response to increasing amounts of the ligand.[11]

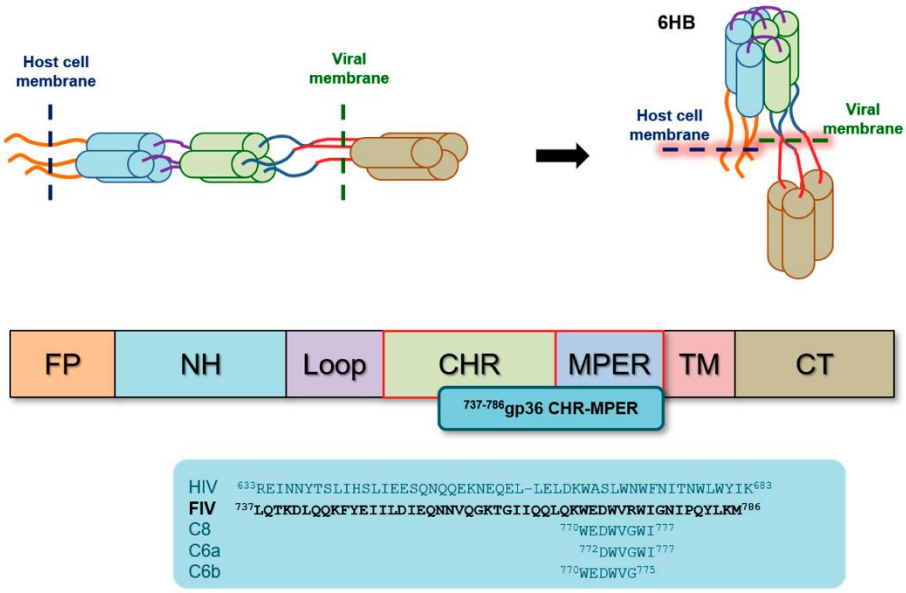

Figure 1. Schematic diagram of HIV-1 gp41 and FIV (gp36) which regulated by Envelope glycoprotein and Amino acid sequences of HIV (gp41) and FIV (gp36) N-terminal, Loop, CHR and MPER (membrane-proximal external region).[13]

3.2 C20 conformational analysis

C20 conformational analysis was performed by CD and NMR spectroscopies in bio-membrane mimicking systems consisting of sodium dodecyl sulfate (SDS) micelle solutions. Surfactants, such as zwitterionic dodecyl phosphocholine (DPC) or negatively charged SDS, are used to make micelles at considerably higher concentrations than their critical micelle concentration (c.m.c.).[15-17] The polar headgroups of these surfactants are found on the surface, and the hydrophobic tails point to the center, forming spherical aggregates. Micelle solutions are widely used as biomimetic membrane systems to study the structural properties of membranotropic molecules. From the technical point of view, they represent ideal systems for CD and NMR analysis in solution, as they tumble sufficiently quickly to result in high-

resolution spectral lines.

3.2.1. Sample preparation: peptide synthesis

C20 peptide characterized by amino acid residue ^{626}AGAGTGATAIGMVTQYHQVL^{645} was synthesized by the Fmoc solid phase synthesis method according to the standard procedure previously published.[18] The peptide purification was done by using HPLC with a C-18 column using 0.1 % aqueous TFA as a buffer A and CH_3CN/H_2O (90:10) with 0.1% TFA as buffer B.

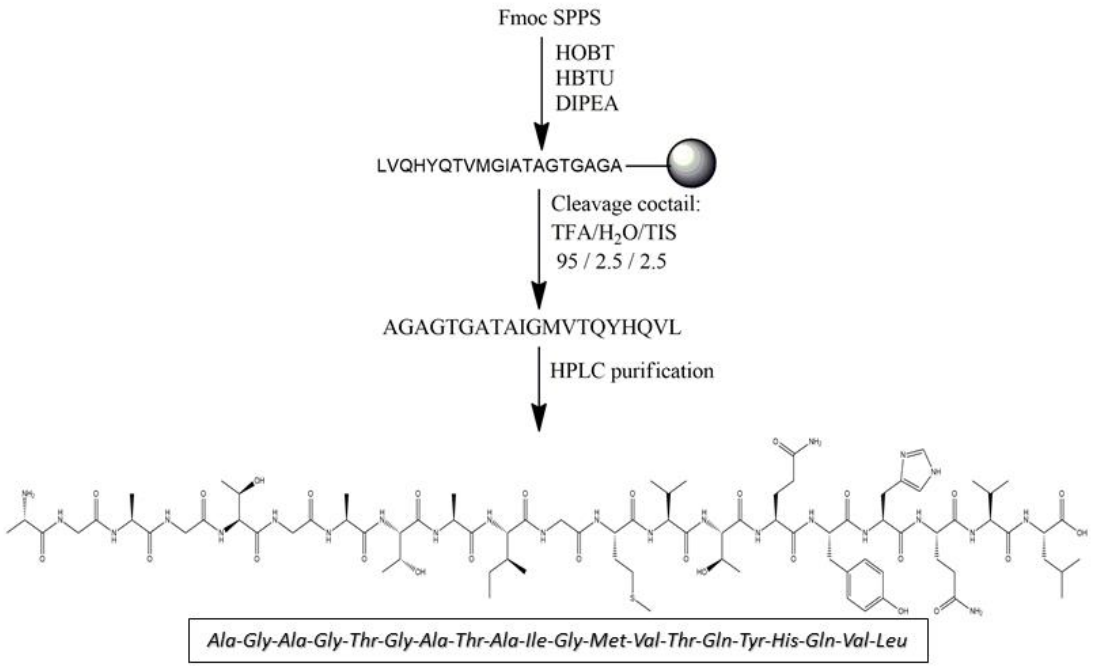

Figure 2: C20 peptide synthesis procedure by solid-phase synthesis protocols.

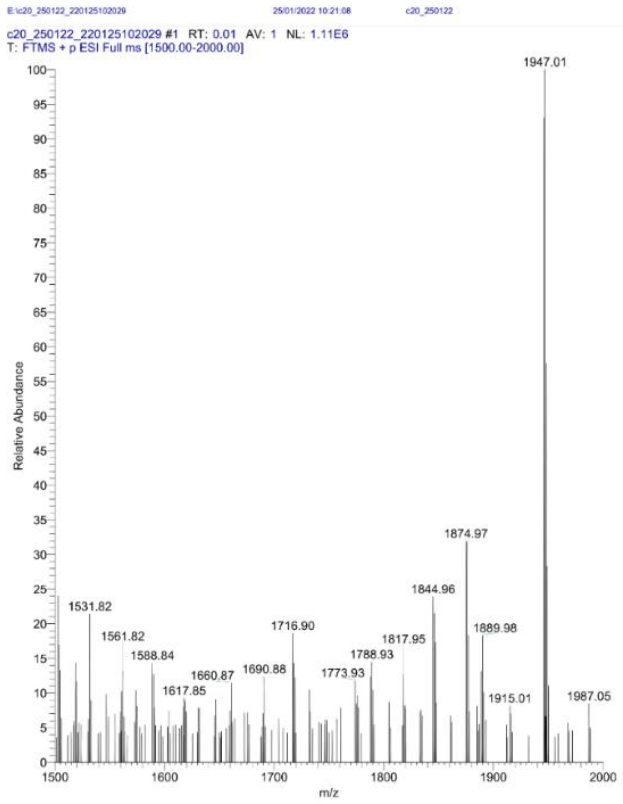

Figure 3 Analysis of crude C20 performed on a Bruker MS-MS.

3.2.2- Circular Dichroism of C20

To have preliminary information on the conformation of C20, CD spectra were recorded in SDS micelle solution. CD spectra were acquired at 2mM, 4mM, 8mM, 80Mm SDS concentrations (**Figure 4**) [19-22]. Quantitative estimation of CD data was performed using the DICHROWEB website with CONTIN and SELCON3 algorithms.[23] According to the shape of CD curves and the quantitative evaluation of CD data, C20 in SDS micelle solution is characterized by a prevalent helical structure. The content of the helical structure increases with the increase of SDS concentration.(**Figure 4**)

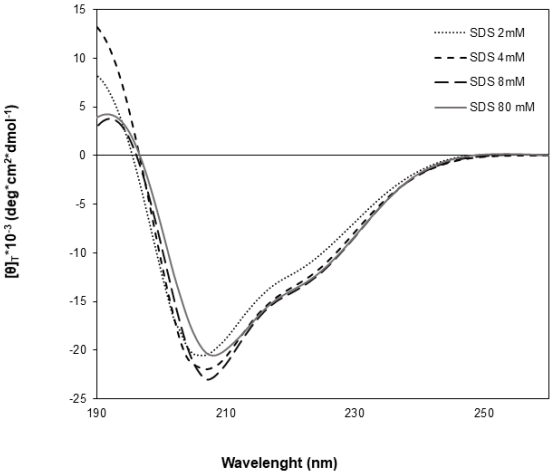

C20/SDS	%α-helix	%β-sheet	%turn	%Randum coil
C20-2mM SDS	81	0	14	5
C20-4mM SDS	91.2	0	8.8	0
C20-8mM SDS	100	0	0	0
C20-80mM SDS	90.1	0	9.9	0

Figure 4: Normalized circular dichroism (CD) spectra of C20 in 2mM, 4mM, 8mM and 80mM SDS concentration. The CD spectra were acquired using a JASCO J810 spectropolarimeter at room temperature with a cell path length of 1 mm. The measurement range spans from 190 to 260 nm.

3.2.3 NMR Structure Spectroscopy

NMR spectra of C20 in 80 mM SDS micelle solution were recorded on a Bruker DRX-500 spectrometer. Chemical shift assignments of the proton spectra were achieved via the standard systematic application of 2-D TOCSY and NOESY experiments using the SPARKY software package (**Figure 5**).[24] according to the procedure of Wüthrich.[25-28] The values of the proton chemical shifts are reported in Table 1. NOE-derived restraints were extracted from NOESY spectra and transformed in interprotonic distances to calculate C20 NMR structures by simulated annealing calculations and using CYANA software (**Figure. 7**). The best 50 NMR structures selected according to the lowest values of the target function were energy minimized, using the distance restraints with a progressively lower force constant (**Figure. 5**).[7] Analysis of dihedral angles using the PROMOTIF program [29] indicates that in SDS micelles (**Figure. 6**), C20 assumes α-helical conformation on the residues Gly6-Ile10. Less regular turn helical structures are in the remaining segments of the sequence.

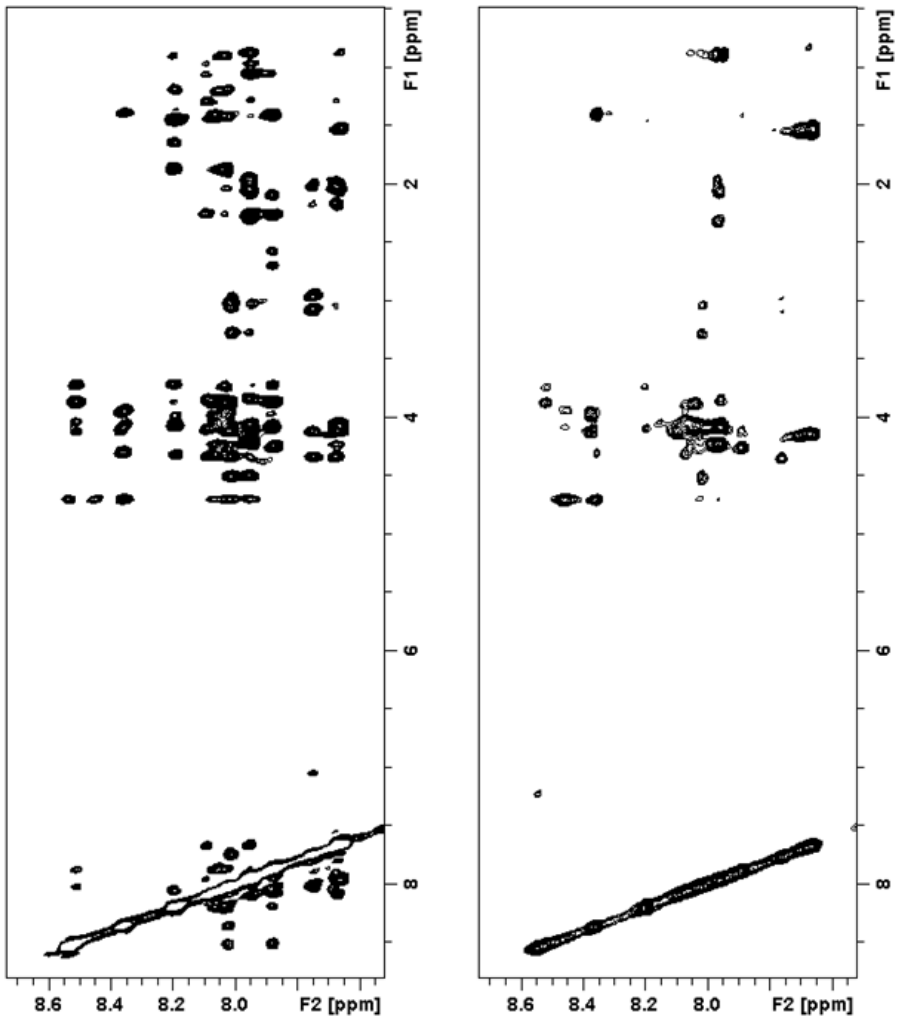

Figure 5: Low field region of the NOESY and TOCSY spectra of C20 in SDS (80 mM) micelle solution. Spectra were recorded at 500MHz and 300K.

Table I: 1H chemical shift of C8 in SDS micelle solution

Residue number	Residue name	HN	Hα	Hβ	Hγ	Others
1	ALA					
2	GLY	8.457	Hα2: 4.076 Hα3: 3.925			
3	ALA	8.356	4.294	1.381		
4	GLY	8.368	Hα2: 4.093 Hα3: 3.946			
5	THR	8.069	4.116	4.029	Qγ2: 1.186	

6	GLY	8.514	Hα2: 3.860 Hα3: 3.707			
7	ALA	7.882	4.083	Qβ: 1.397		
8	THR	8.065	4.307	3.99	Qγ2: 1.199	
9	ALA	8.193	4.076	Qβ: 1.439		
10	ILE	8.193	3.713	1.863	Hγ12: 1.635 Hγ13: 1.174 Qγ2: 0.894	Qδ1: 0.820
11	GLY	8.032	Qα: 3.866			
12	MET	7.879	4.244	Hβ2: 2.291 Hβ3: 0.054	Hγ2: 2.693 Hγ3: 2.569	
13	VAL	7.949	3.831	2.254	Qγ1: 1.054 Qγ2: 0.962	
14	THR	8.089	4.326	4.103	Qγ2: 1.275	
15	GLN	7.693	4.121	Qβ: 2.015	Qγ: 2.163	Hε21: 7.282
16	TYR	7.747	4.329	Hβ2: 3.065 Hβ3: 2.958		Qδ: 7.049 Qε: 6.721
17	HIS	8.01	4.497	Hβ2: 3.264 Hβ3: 3.024		Hδ1: 7.197 Hδ2: 7.202 Hε1: 7.045
18	GLN	7.956	4.215	Hβ2: 2.031 Hβ3: 1.935	Qγ: 2.291	Hε21: 7.445
19	VAL	7.958	4.054	2.039	Qγ2: 0.867	
20	LEU	7.668	4.117	Qβ: 1.513		Qδ1: 0.849 Qδ2: 0.802

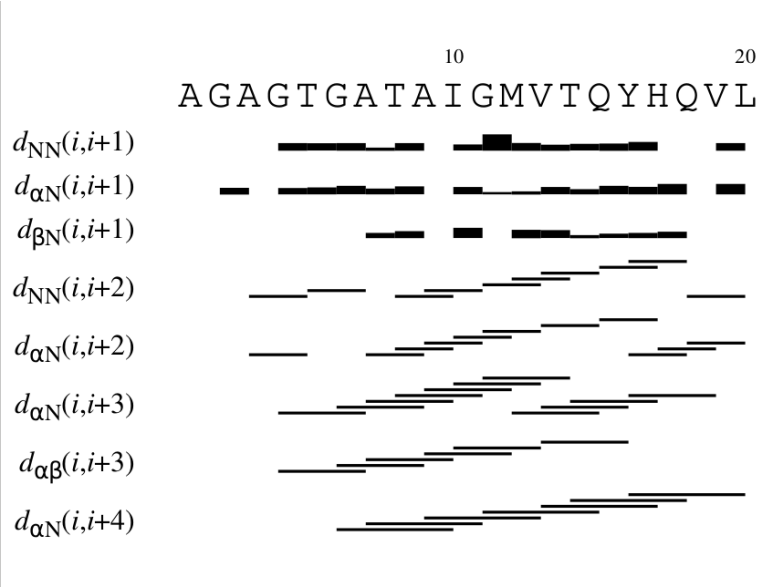

Figure 6: Sequential and medium-range connectivity collected in NOESY spectra of C20 in SDS micelle solution.

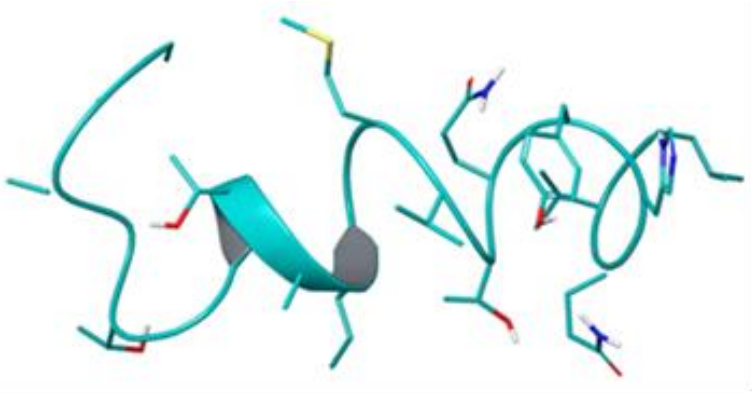

Figure 7: Best NMR structure of C20 in SDS solution. The model was derived by simulating annealing using CYANA software.

3.2.4 Molecular Dynamics

The structure of a Gp36 construct corresponding to CHR-MPER was previously solved in our lab using 2D and 3D NMR experiments.[13] CHR-MPER includes 2 α-helix segments connected by a flexible loop regulating helix orientation at circa forty-degree angle. Molecular dynamics simulations (39 ns. using GROMACS and CHARMM36 force field), including C20 peptide in complex with CHR-MPER, were carried out in explicit water to investigate the

potential interaction of C20 with CHR-MPER [30, 31]. Trajectory file was saved using *gmx trjconv* tool included in GROMACS package. **Figure 8,** showing the superimposition of all the frames from the simulation, indicates that the complex formed by the peptide and 737-786gp36 CHR–MPER is stabilized by a high number of interactions (**Table 2, Figure 9**). In particular, the bonds plot (**Figure 10a**) calculated from the trajectory reports many of H-bonds and non-bonded interactions within 0.35 nm established between the C20 peptide and 737-786gp36 CHR–MPER. Interestingly, the graph reporting energies from short-range electrostatic interactions (**Figure 10b**) outlines a clear point where the two interacting peptides reach an energy minimum that corresponds to the stabilization of the complex. The simulation shows that a strong interaction occurs between the two peptides. Interestingly, analysis of interactions indicates that C20 has a propensity to bind the residues corresponding to the gp36 CHR. This result reproduces the biological condition: indeed C20 is part of gp36 NHR [14], which is known to have a strong affinity for CHR in the formation of the hairpin-like conformation in the 6HB.

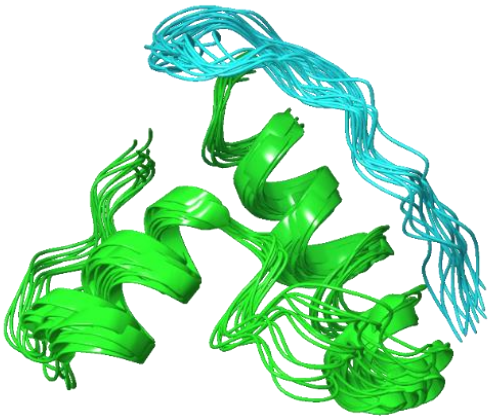

Figure 8. 3D coordinates derived from MD trajectory of the 39 ns simulation between $^{737\text{-}786}$gp36 CHR–MPER (green ribbons) and C20 (cyan ribbons).

Table 2. Interactions between $^{737\text{-}786}$gp36-CHR-MPER and C20 as resulting from the last frame in the trajectory obtained from 39 ns MD simulation.

$^{737\text{-}786}$gp36-CHR-MPER	Interaction	C20
Leu 737	Cation-π stacking	Tyr 16
Thr 739	H-bond	Val 13
Gln 743	H-bonds	Gln 15, His 17
Glu 754	Salt bridge	Ala 1
Glu 754	H-bond	Gly 2
Gln 755	H-bonds	Gly4
Met 786	H-bonds	Gly 11, Met 12

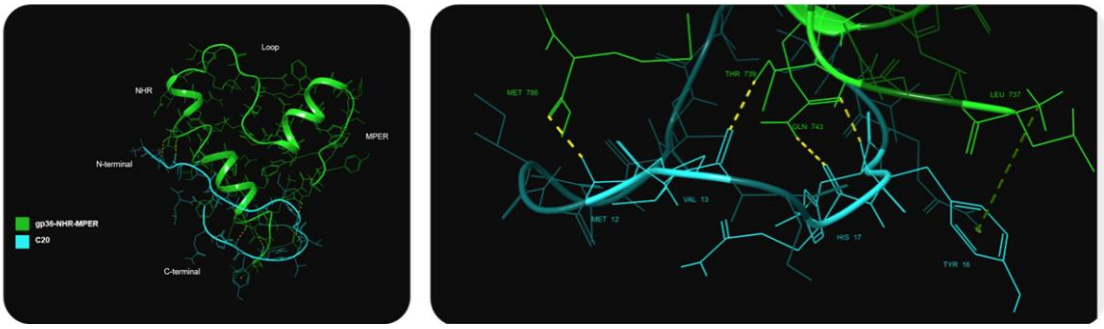

Figure 9. The structures of 737-786 CHR-MPER fit the pharmacophore model of C20. Dashed lines show the distances in Å between the key functional moieties.

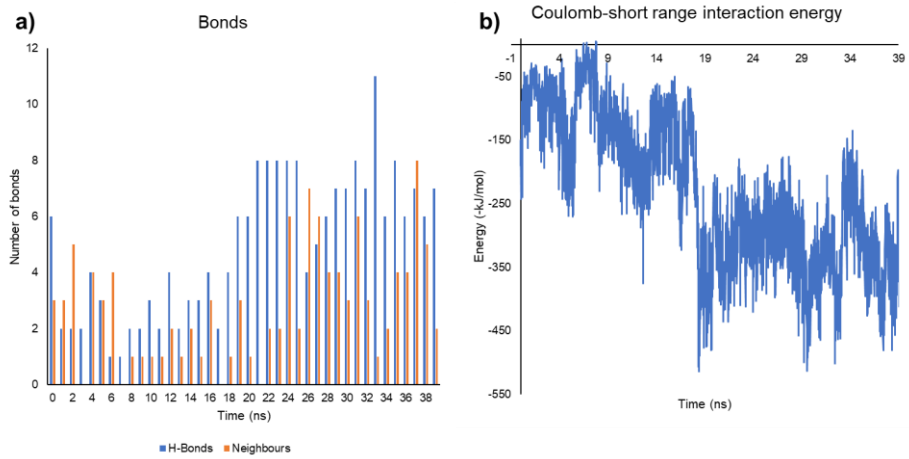

Figure 10. Graphs reporting **a)** number of bonds (H-bonds and neighbour contacts within 0.35 nm) and **b)** Coulomb short-range interaction energies plotted against the time obtained from 39 ns MD simulations of $^{737\text{-}}$

^{786}gp36 CHR–MPER and C20.

3.3 Conclusion

In this part of my Ph.D. research activity, I synthesized and performed NMR conformational analysis of C20 in SDS micelle solution. This represents the first step of an investigation aimed at characterizing the potential interaction of C20 with other regions of Gp36, particularly CHR-MPER. Our data show the preference of C20 to assume turn-helical structure along the whole sequence with a short segment of regular α-helix in the central part of the sequence. Furthermore, molecular dynamics calculation indicates that C20 forms a stable structural complex with CH-MPER, establishing interactions mainly with the CHR portion. This is consistent with the nature of the C20 sequence, originally selected as part of Gp41 NHR and designed to interact with the CHR counterpart.

3.4 Material and Methods

3.4.1 Synthesis of C20

The C20 peptide with amino acid residue ^{627}AGAGTGATAIGMVTQYHQVL^{646} was synthesized manually using Fmoc solid-phase synthesis [15] acidic resin (Wang) 200 mg (1.1 mmol/g). The resin was swelled in DMF for 2 h at room temperature, then was washed with DMF (2× 20s with 2 mL). Afterward, to continue the amino acid chain, we added to resin 4 equiv. of HOBT and HBTU, and DIPEA as coupling reagents to make the coupling. Deprotection of the Fmoc group was affected with 20% piperidine in DMF (**Figure2**). Following synthesis, the peptide resin it was then washed thoroughly with DMF and DCM and then lyophilized.

To cleave the peptide from the resin and remove all protecting groups, we used a cleavage cocktail solution containing (TFA/H_2O/TIS (95: 2.5: 2.5), 3 mL) for 2 h. After that we collected the filtered solution and washed the reagent twice with the same cleavage cocktail (1mL) for 30s. TFA was removed by evaporation and the product precipitated in ether. Next, the product

was washed with ether (3-2 mL) and we later removed the ether and the crude product, dried and lyophilized before. To analyze the product, we used preparative HPLC, which was done on a C-18 column using 0.1 % aqueous TFA as a buffer A and CH_3CN/H_2O (90:10) with 0.1% TFA as buffer B. After collecting the fraction, the main compound and its purity were confirmed by MS/MS (**Figure.3**).

3.4.2 Circular Dichroism of C20

CD experiments were performed at 25°C on an 810-Jasco spectropolarimeter, working on average of 4 scans with 10 nm/min scan speed, 4 s response time, and 2 nm bandwidth. We used a quartz cuvette with a path length of 1 mm, a measurement range from 190 to 260 nm (far UV). Throughout the measurements, we ensured a voltage lower than 700 V, which guarantees the reliability of the obtained data.

Fig2. shows CD spectra collected on samples containing C20 peptide ($5.0 \times 10{-}4$ M) in a solution containing increasing amounts of SDS (from 2 to 80 mM concentration) and The concentrations of SDS and DPC which was 10:90 respectively. (**Figure 4**) shows that the shapes of the CD spectra vary in dependence of lipid composition. Quantitative analysis of CD curves, using CONTIN algorithm (DICHROWEB), indicates that in a solution containing an excess of SDS detergent, C20 assumes 100% helical structure. In contrast, in a solution containing lower amounts of SDS detergent, decreasing helical structure content are observable and in SDS/DPC solution was agregate.

3.4.3 NMR Structure Spectroscopy

NMR spectra were recorded on a Bruker DRX-600 spectrometer and acquired in the same SDS mixture used for the CD measurement, but using 0.1 mM peptide concentration. To exclude potential aggregation, we recorded the 1D proton spectra at a concentration range

spanning 1- 0.1 mM. Qualitative and quantitative analyses of 3D NMR spectra were achieved via the standard systematic application of 2-D TOCSY and NOESY experiments using the SPARKY software. To assigned chemical shift values of backbone ^{15}N, $^{13}C\alpha$, and $^{13}C'$ were used as input for the TALOS+ program [32] to predict backbone dihedral angles.

3.5.4 Molecular dynamics

Molecular Dynamics (MD) simulations on C20 structure obtained from CYANA calculations were performed with GROMACS [33, 34] by using CHARMM36 force field.[31] The simulations were run for 39 ns at 300 K. The structure was immersed in explicit water using the TIP4P model. The protein was solvated, and the system was neutralized by adding 3 Na^+ ions. After these steps, the energy minimization of the system was performed, and then the system was equilibrated using NVT and NPT runs. The system's temperature and pressure were kept constant at 300 K and 1.01325 bar using the Berendsen weak coupling method.[35, 36] The results were used for a 50 ns MD simulation using Particle Mesh Ewald for long-range electrostatics under NPT conditions.[37] The trajectory file was fitted in the box and converted in PDB coordinates by using *trjconv* tool of GROMACS Package. The structure was visualized with Maestro by Schrödinger.[38] Number of H-bonds and neighbours within 0.35 nm were calculated using *hbond* tool of GROMACS. Coulomb short-range interaction energies were calculated using *energy* tool of GROMACS.

3.5 References

1. Frey, S.C., E.A. Hoover, and J.I.J.J.o.v. Mullins, *Feline immunodeficiency virus cell entry.* 2001. **75**(11): p. 5433-5440.
2. Wyatt, R. and J.J.S. Sodroski, *The HIV-1 envelope glycoproteins: fusogens, antigens, and immunogens.* 1998. **280**(5371): p. 1884-1888.
3. Harrison, S.C.J.N.s. and m. biology, *Viral membrane fusion.* 2008. **15**(7): p. 690-698.
4. Sackett, K. and Y.J.B. Shai, *The HIV-1 gp41 N-terminal heptad repeat plays an essential role in membrane fusion.* 2002. **41**(14): p. 4678-4685.
5. Wild, C.T., et al., *Peptides corresponding to a predictive alpha-helical domain of human immunodeficiency virus type 1 gp41 are potent inhibitors of virus infection.* 1994. **91**(21): p. 9770-9774.
6. Pellecchia, M., et al., *Perspectives on NMR in drug discovery: a technique comes of age.* Nature Reviews Drug Discovery, 2008. **7**(9): p. 738-745.
7. Peng, J.W., J. Moore, and N. Abdul-Manan, *NMR experiments for lead generation in drug discovery.* Progress in Nuclear Magnetic Resonance Spectroscopy, 2004. **44**(3-4): p. 225-256.
8. Goldflam, M., et al., *NMR Studies of Protein-Ligand Interactions.* Protein Nmr Techniques, Third Edition, 2012. **831**: p. 233-259.
9. Medek, A., et al., *The use of differential chemical shifts for determining the binding site location and orientation of protein-bound ligands.* Journal of the American Chemical Society, 2000. **122**(6): p. 1241-1242.
10. Krishnamoorthy, J., V.C.K. Yu, and Y.-K. Mok, *Auto-FACE: An NMR Based Binding Site Mapping Program for Fast Chemical Exchange Protein-Ligand Systems.* Plos One, 2010. **5**(2).
11. Reibarkh, M., T.J. Malia, and G. Wagner, *NMR distinction of single- and multiple-mode binding of small-molecule protein ligands.* Journal of the American Chemical Society, 2006. **128**(7): p. 2160-2161.
12. Grimaldi, M., et al., *Structural basis of antiviral activity of peptides from MPER of FIV gp36.* PLoS One, 2018. **13**(9): p. e0204042.
13. Grimaldi, M., et al., *NMR Structure of the FIV gp36 C-Terminal Heptad Repeat and Membrane-Proximal External Region.* Int J Mol Sci, 2020. **21**(6).
14. Giannecchini, S., et al., *Antiviral activity and conformational features of an octapeptide derived from the membrane-proximal ectodomain of the feline immunodeficiency virus transmembrane glycoprotein.* J Virol, 2003. **77**(6): p. 3724-33.
15. Mannhold, R., H. Kubinyi, and G. Folkers, *BioNMR in drug research*. 2006: John Wiley & Sons.
16. Pandey, S., et al., *Designed glucopeptides mimetics of myelin protein epitopes as synthetic probes for the detection of autoantibodies, biomarkers of multiple sclerosis.* 2012. **55**(23): p. 10437-10447.
17. Zerbe, O., et al., *BioNMR in drug research*. Vol. 25. 2003: Wiley-VCH Zurich.
18. Kwon, B., et al., *Oligomeric structure and three-dimensional fold of the HIV gp41 membrane-proximal external region and transmembrane domain in phospholipid bilayers.* 2018. **140**(26): p. 8246-8259.
19. Scott, R.E., et al., *Plasma membrane vesiculation in 3T3 and SV3T3 cells. I. Morphological and biochemical characterization.* Journal of Cell Science, 1979. **35**(1): p. 229-243.
20. Del Piccolo, N., et al., *Production of plasma membrane vesicles with chloride salts and their utility as a cell membrane mimetic for biophysical characterization of membrane protein interactions.* Analytical chemistry, 2012. **84**(20): p. 8650-8655.
21. Scott, R.E. and P.B. Maercklein, *Plasma membrane vesiculation in 3T3 and SV3T3 cells. II. Factors affecting the process of vesiculation.* Journal of Cell Science, 1979. **35**(1): p. 245-252.
22. Scott, R.E., *Plasma membrane vesiculation: a new technique for isolation of plasma membranes.* Science, 1976. **194**(4266): p. 743-745.
23. Whitmore, L. and B.J.N.a.r. Wallace, *DICHROWEB, an online server for protein secondary structure analyses from circular dichroism spectroscopic data.* 2004. **32**(suppl_2): p. W668-W673.
24. Goddard, T. and D.J.G.S.T.i.n.c.r.f.t.r. Kneller, *Sparky 3; University California, San Francisco; 2004.* 2021.
25. Jeener, J., et al., *Investigation of exchange processes by two-dimensional NMR spectroscopy.* 1979. **71**(11): p. 4546-4553.
26. Piantini, U., O. Soerensen, and R.J.C.I. Ernst, *Multiple Quantum Filters for Elucidating NMR*

Coupling Networks (Anwendung auf die Anregung von 1, 3-Dibrom-butan). 1983. **14**(9): p. no-no.

27. Bax, A. and D.G.J.J.o.M.R. Davis, *MLEV-17-based two-dimensional homonuclear magnetization transfer spectroscopy.* 1985. **65**(2): p. 355-360.

28. Wüthrich, K.J.E.N., *NMR with proteins and nucleic acids.* 1986. **17**(1): p. 11-13.

29. Hutchinson, E.G. and J.M.J.P.S. Thornton, *PROMOTIF—a program to identify and analyze structural motifs in proteins.* 1996. **5**(2): p. 212-220.

30. Abraham, M.J., et al., *GROMACS: High performance molecular simulations through multi-level parallelism from laptops to supercomputers.* 2015. **1**: p. 19-25.

31. Huang, J. and A.D.J.J.o.c.c. MacKerell Jr, *CHARMM36 all-atom additive protein force field: Validation based on comparison to NMR data.* 2013. **34**(25): p. 2135-2145.

32. Shen, Y., et al., *TALOS+: a hybrid method for predicting protein backbone torsion angles from NMR chemical shifts.* 2009. **44**(4): p. 213-223.

33. Bekker, H., et al., *Gromacs: A parallel computer for molecular dynamics simulations.* 1993.

34. Abraham, M.J., et al., *GROMACS: High performance molecular simulations through multi-level parallelism from laptops to supercomputers.* SoftwareX, 2015. **1**: p. 19-25.

35. Berendsen, H.J., et al., *Interaction models for water in relation to protein hydration*, in *Intermolecular forces*. 1981, Springer. p. 331-342.

36. Bussi, G., D. Donadio, and M. Parrinello, *Canonical sampling through velocity rescaling.* The Journal of chemical physics, 2007. **126**(1): p. 014101.

37. Onufriev, A., D.A. Case, and D. Bashford, *Effective Born radii in the generalized Born approximation: the importance of being perfect.* Journal of computational chemistry, 2002. **23**(14): p. 1297-1304.

38. Schrödinger, *Maestro*. 2020, LLC: New York, NY.

4. Design and synthesis of new peptides and peptidomimetic deriving from Gp36 sequence.

4.1 Introduction

The conformational transition of Gp41 and Gp36 to promote entry of HIV or FIV in the host cell can be effectively blocked by peptides that simulate preserved functional elements in Gp41 or Gp36. A well-known model of such peptides, termed fusion inhibitors, is the peptide T-20 (enfuvirtide, Fuzeon), which is utilized as rescue therapy for HIV/AIDS.[1]

In the search for molecules that act as antiviral agents by inhibiting the formation of the six-helix bundle (6HB) of Gp36, which is required for viral entry, we previously identified an eight-amino acid peptide containing such a Trp motif (770W-I777), designated C8. This peptide had potent antiviral activity on all FIV isolates tested, with activity dependent on an intact Trp motif. To gain information relevant to the rational design of modified peptides, extensive structure-activity relationship studies were performed.[2-6] Based on conformational data that showed the importance of Trp side chain alignment for C8 activity, a C8 retro-inverso analog with unmodified C8 antiviral activity was synthesized in vivo.[7]

With the aim of expanding the study of Gp36-derived peptides, part of my PhD research, particularly the part conducted at the Department of Drug Design and Pharmacology, College of Copenhagen, was aimed at synthesizing i) new C8 analogs and ii) new Gp36-derived peptides based on the results of a computational epitope mapping approach.

4.2 New C8 analogs

4.2.1 Cyclic C8

The interest of the scientific community and the pharmaceutical industry has always been

focused on peptide molecules as therapeutic agents. In principle, the use of peptides could be advantageous for many reasons: they are highly biomimetic as substitutes for endogenous molecules, are easy to synthesize, are non-toxic, and could meet the conformational requirements for high and specific biological activity.[8] However, several drawbacks have prevented their use as therapeutics for a long time: i) peptide medicines have limited oral absorption, for which injection is the most common method of delivery. ii)even after effective absorption, proteolytic enzymes quickly metabolize peptides. Finally, iii) peptides often have difficulty crossing the cell membrane.

One of the main concerns when testing a peptide, particularly a short one, as a drug candidate is its conformational flexibility and enzymatic stability, making its half-life in serum too short for therapeutic application. Based on the idea that reduced conformational flexibility may be advantageous for C8 antiviral activity, we decided to synthesize its cyclic analog.

Chemists have been increasingly adept in designing peptide analogs resistant to metabolism while maintaining significant biological activity.[9] Peptide cyclization generally improves the selective binding and stability of linear precursors; however, not all cyclization strategies and constrained geometries enhance these properties to the same extent. From a conformational point of view, cyclization increases the propensity for β-turn formation in peptides. On the other hand, the formation of this secondary structure is significant since β-turns are often found in native proteins.[10]

Numerous pharmacologically active peptides, both natural and synthetic, are characterized by cyclic ring structures. Several chemical bonds, such as amide, lactone, ether, thioether, and disulfide, can be used to attach one end to the other to produce a ring structure.

A head-to-tail (or N-to-C) cyclic peptide is formed when amide bonds form between the amino and carboxyl termini. There are several biologically active N-to-C cyclic peptides in nature.[11] Because of their structural stiffness, cyclic peptides usually exhibit increased biological activity than their linear counterparts[12]; also, the entropy term of the Gibbs free

energy is reduced by the stiffness of cyclic peptides, allowing for increased binding toward target molecules or receptor selectivity. Another advantage of the cyclic structure is its resistance to exopeptidase hydrolysis due to the absence of amino and carboxyl termini. Because their structure is less flexible than linear peptides, cyclic peptides can be resistant to endopeptidases. Some, but not all, cyclic peptides can pass the cell membrane.[9, 13]

With the intent of taking advantage of all the properties of the cyclo peptides and inspired by the potent antiviral activity of C8 and by the peculiar biophysical behavior of the peptide, we decided to synthesize the cyclic C8 analog to evaluate the effect deriving from structural stiffening on its biological and biophysical properties. In particular, we decided to use a head-to-tail cyclization procedure to avoid amino acid substitutions in C8 sequences that could intact the original structural properties of the peptide.

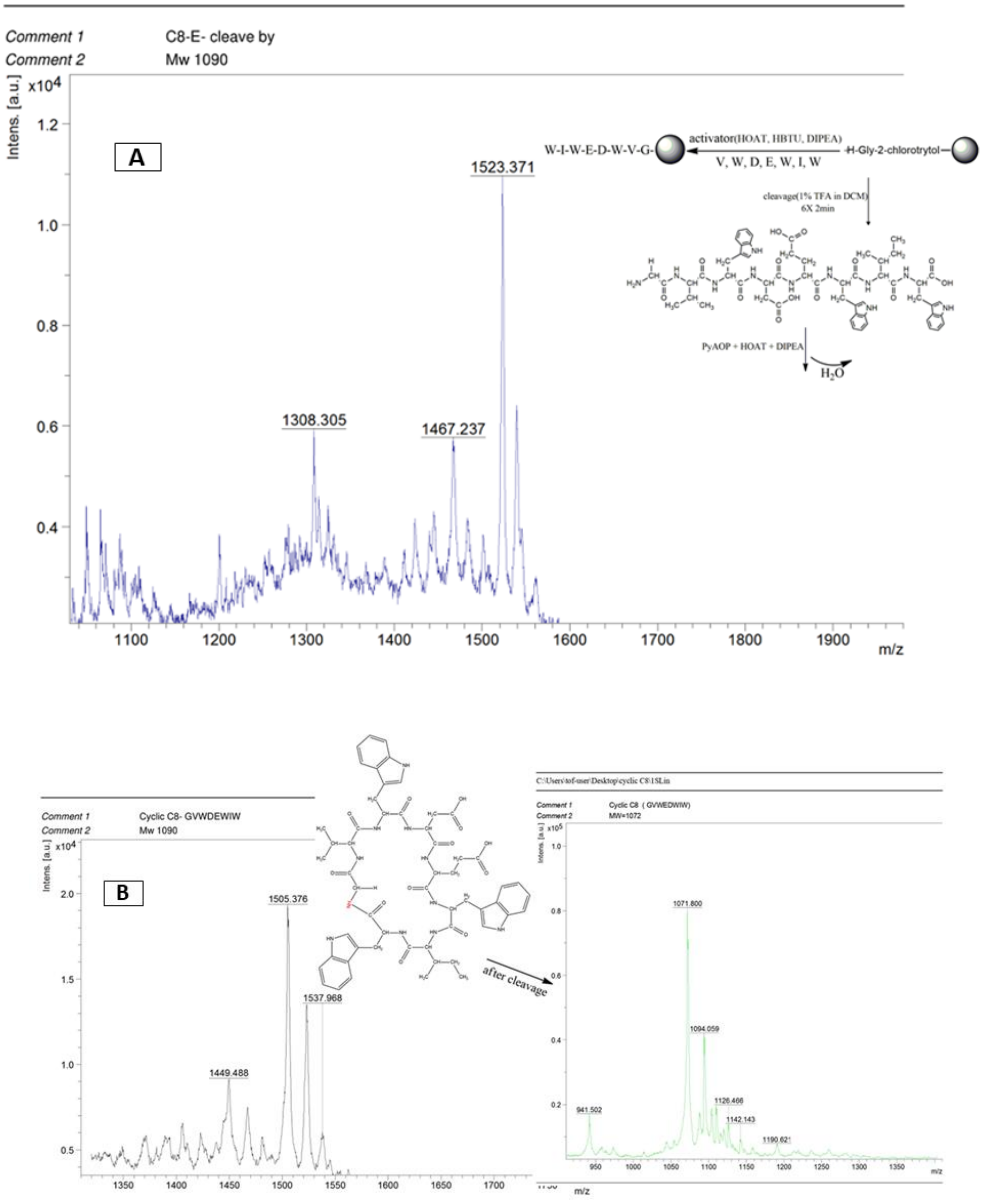

Figure 1 A. Linear C8 synthesis analysis. **B**.Cyclic C8 analogs synthesized by solid phase peptide synthesis.

4.2.2 C8 Peptoid

As pharmacological agents, peptides have well-known drawbacks, the most serious of which are protease sensitivity and poor cell permeability. Therefore several distinct forms of peptidomimetics have been studied in the hopes of discovering a family of chemicals that have the same protein-binding properties as peptides but have better pharmacokinetic features. Peptidoids are regarded as peptide-mimetics with a wide range of biological applications, Because of their proteolytic stability and structural diversity.

Peptoids with a dominant balanced hydrophobic and charge distribution throughout the backbone have been explored in several biological systems. Tryptophan is an essential amino acid found in many biologically active peptides. Tryptophan-like side chains in peptoids Due to the peculiar indole ring allow H-bonding, which is absent from the parent backbone. Moreover, the rigid hydrophobic core and the bulky nature of tryptophan and hydrogen-bonding potential allows accommodating tryptophan-like side chains into the interfacial regions of bacterial membranes and causing bacterial membrane damage.[14, 15]

The researchers used peptoids as a model system and discovered that N-alkylated species are up to 20 times more cell-permeable than similar peptides. These findings show that peptoids could be valuable reagents for targeting intracellular proteins, in addition to their other advantages.[16-18]

In order to improve the pharmacokinetic properties of C8 and at the same time understand the structural requirements necessary for its antiviral activity, C8 analogs were previously synthesized by systematically replacing Trp residues. Furthermore, the amino acids between the Trp residues were replaced by simple alkyl spacers of appropriate length. As a result, simpler hexapeptides almost entirely made up of unnatural amino acid residues showed increased enzymatic stability while maintaining strong antiviral potency in vitro.[7] Further exploring the possibility of identifying C8 analogs endowed with improved pharmacodynamic and pharmacokinetic properties, we decided to synthesize new peptoid C8 analogs characterized by replacing Trp residue with tryptamine.

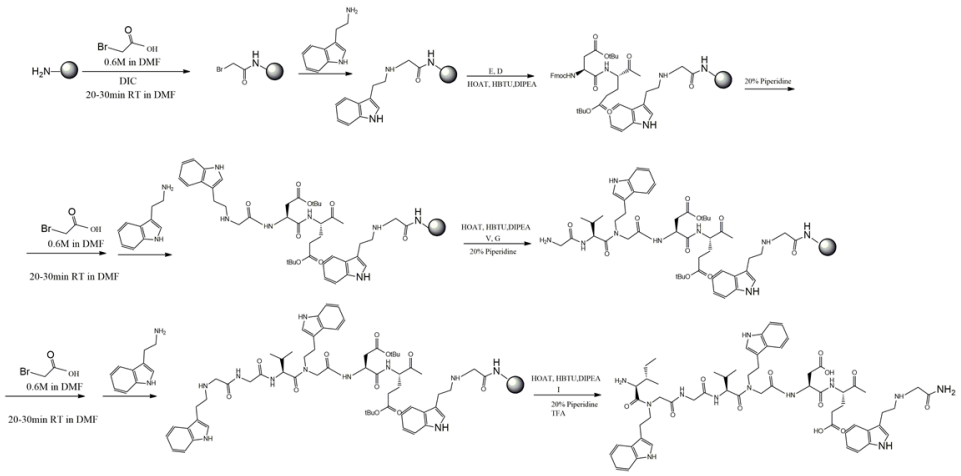

Figure. 2 C8 peptoids rich in Ntrp synthesis by solid phase submonomer peptoid synthesis protocols.

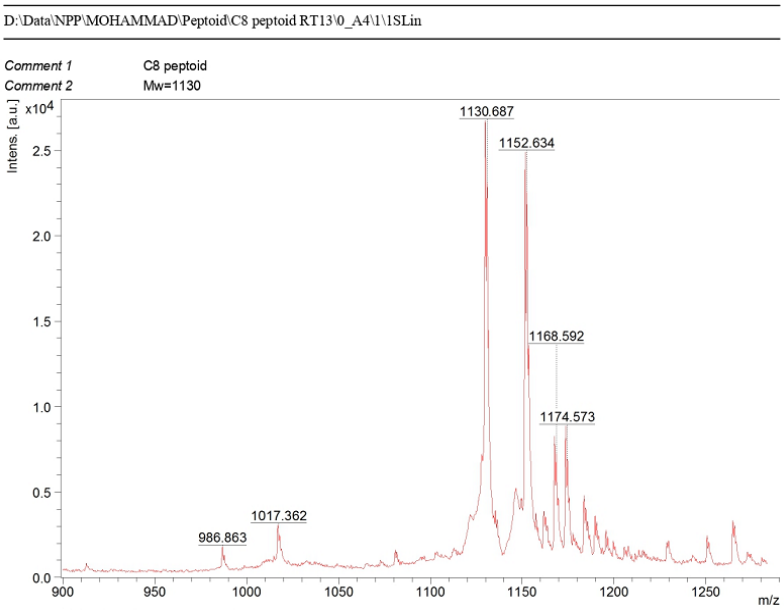

Figure 3. Maldi Mass chromatograms of C8 peptoid modified with Nhtrp synthesized using automated solid-phase synthesizer.

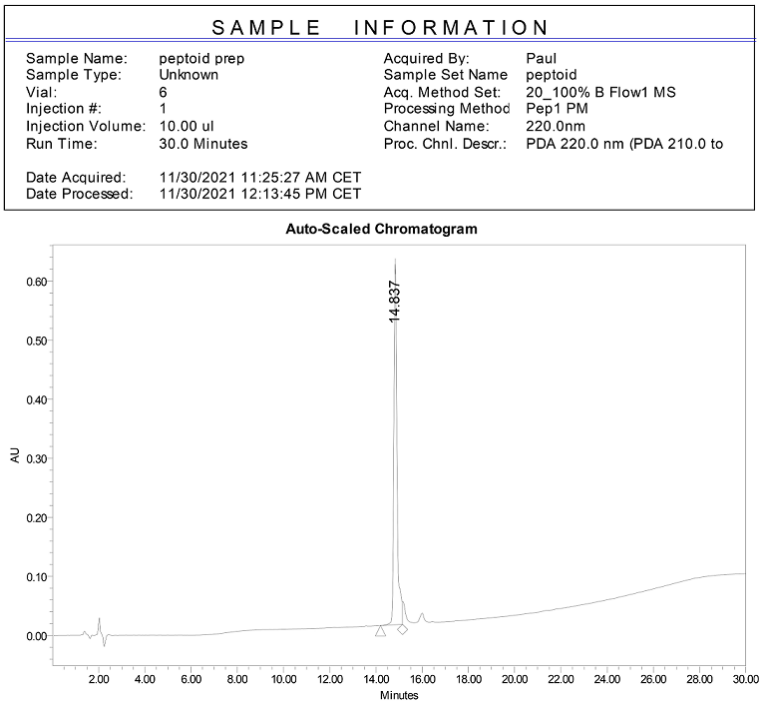

Figure 4. Analytical HPLC chromatograms of prep C8 peptoid to confirm the purity in 20-100% of solvent B.

4.3 Results

4.3.1 Cyclic peptide synthesis

Peptides were synthesized via standard Fmoc/tBu SPPS on 2-chlorotrityl resin and then released in mildly acidic conditions (TFE/DCM). The crude product was then dissolved in DMF for the ring-closure reaction, for which PyAOP was used as coupling reagent.[25]

4.3.2 C8 Peptoid synthesis

C8 Peptoid (Figure 2) was synthesized using standard submonomer solid-phase synthesis on TantaGel resin.[15]

4.3.3 Epitope map Scanning

4.3.3.1 Epitope Map Scanning of FIV envelope GP36

To identify new peptides with anti-FIV effect, part of my research activity was focused on the epitope map scanning of FIV gp36 sequence from FP-MPER.

Considering that gp36, as gp41 in HIV, undergo to conformational rearrangements stabilized by the intramolecular interaction of different segments of the protein, we decided to perform a computer-based epitope map scanning to find short segments of gp36 able to bind with high-

affinity Gp36 in a specific region. In detail, gp36 residues 616-786 (**Figure 5**, including Gp36 regions from FP to MPER) were mapped by dividing the sequence every 10 amino acids and overlapping the last 5 amino acids to the subsequent ones. Thus every peptide included the last half of the previous. This way, we obtained a library of 33 decapeptides (**Table 1**). Then we decided to perform a molecular docking-based screening using the 3D gp36 structure built as a target protein using homology modeling from the coordinates of Gp41 cristal structure.

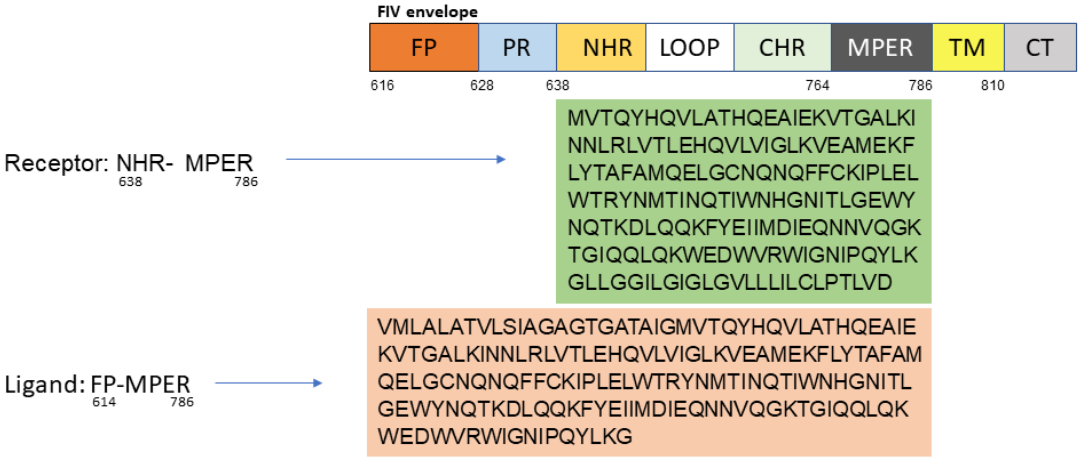

Figure.5 structural framework and conformational rearrangement of FIV (gp36) which regulated by Envelope glycoprotein and Amino acid sequences of FIV (gp36) Fusion peptide (FP), PR, N-terminal, Loop, CHR and MPER (membrane-proximal external region)

Table.1 Selection of 10 amino acid long sequences of FIV envelope gp36 from (Fusion peptide (FP), PR, N-terminal, Loop, CHR and MPER (membrane-proximal external region) with 5 amino acids overlapping.

1- VMLALATVLS	2- ATVLSIAGAG	3- IAGAGTGATA	4- TGATAIGMVT	5- IGMVTQYHQV
6- QYHQVLATHQ	7- LATHQEAIEK	8- EAIEKVTGAL	9- VTGALKINNL	10- KINNLRLVTL
11- RLVTLEHQVL	12- EHQVLVIGLK	13- VIGLKVEAME	14- VEAMEKFLYT	15- KFLYTAFAMQ
16- AFAMQELGCN	17- ELGCNQNQFF	18- QNQFFCKIPL	19- CKIPLELWTR	20- ELWTRYNMTI
21- YNMTINQTIW	22- NQTIWNHGNI	23- NHGNITLGEW	24- TLGEWYNQTK	25- YNQTKDLQQK
26- DLQQKFYEII	27- FYEIIMDIEQ	28- MDIEQNNVQG	29- NNVQGKTGIQ	30- KTGIQQLQKW
31- QLQKWEDWVR	32- EDWVRWIGNI	33- WIGNIPQYLKG		

In detail, we built by homology modeling, using SWISS-MODEL[19], the 3D gp36 structure considering the residues 638-810 (from NHR to TMD). The crystal structure of HIV-1 Gp41 in complex with Fab (PDB ID: 6DCQ).[7]was used as a template. The derived 3D gp36 structure was then subjected to a 2 ns molecular dynamics simulation in explicit water (GROMACS 2020.3)[20] to have the conformation with the energetic minimum.

The obtained gp36 structure was used as "receptor protein" for the molecular docking simulation performed with HPepDock,[21] setting the grid box on the whole gp36 protein. In addition, the peptides deriving from epitope mapping were set as "ligand peptides," and the peptides C20, C8, C6a, and C6b, whose anti-FIV activity was previously experimentally demonstrated[4, 6, 22], were used as a control in the molecular docking procedures.

As a result of computer-based epitope mapping, the peptide sequences were selected according to the best docking score and energy parameters. Interestingly, computational procedure indicates that the sequences characterized by the best docking scores cluster in two subsets: one targeting the NHR and the other targeting the CHR domain. (**Figure 6**)

Figure 7 shows the four peptide sequences selected according to the lowest docking scores (kcal/mol), energy scores, and interactions they may establish with gp36.

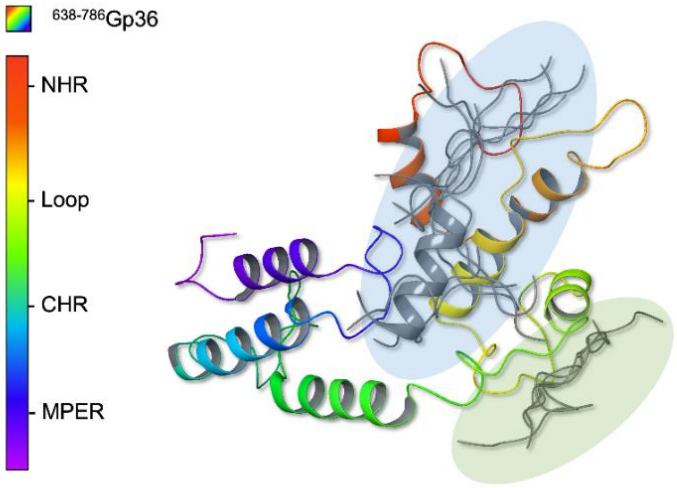

Cluster1	
Peptide	**Docking score (kcal/mol)**
C20	-196.2
C8	-215.1
IGMVTQYHQV	-180.2
QYHQVLATHQ	-208.6
VEAMEKFLYT	-180.4
KFLYTAFAMQ	-212.4
ELWTRYNMTI	-193.1
YNMTINQTIW	-196.9
NQTIWNHGNI	-212.6
EDWVRWIGNI	-198.0
WIGNIPQYLKG	-197.5
Cluster2	
Peptide	**Docking score (kcal/mol)**
C6a	-180.3
KINNLRLVTL	-181.9
RLVTLEHQVL	-184.5
QNQFFCKIPL	-181.8
QLQKWEDWVR	-210.4

Figure 6. Epitope mapping of the gp36: on the left, the protein gp36 (residues 638-786) is represented as rainbow colored ribbon, and the poses of ligand peptides as grey ribbons. The clusters of poses are highlighted in blue and green; on the right are reported the sequences of the ligand peptides with the lowest docking scores (kcal/mol) obtained from HPepDock.

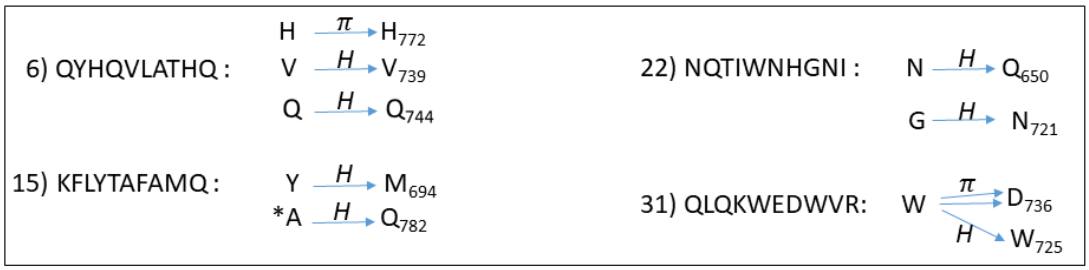

Figure 7. Peptide sequences selected according to epitope map scanning using HPepDock online server. π –π interactions (π) and H bond interactions (H) engaged with the single domain of Gp36 are indicated.

4.3.3.2 Synthesis and purification of peptides from epitope mapping

Based on the reported results, we decided to synthesize the sequences shown in **Figure 7** using Fmoc solid-phase Synthesis according to the previously published procedure.[2] The peptides were synthesized manually using TentaGel resin 200 mg (0.23 mmol/g). The resin was swelled in DMF for 2 h at room temperature. The resin was washed with DMF (2× 20s with 2 mL).

After completing the synthesis, the peptide purity was assessed via reverse-phase analytical HPLC on a system consisting of a Waters 600 pump connected to a Waters Symmetry C18 column and a Waters 2996 PDA detector.

The identity of the peptide was verified by using a Bruker Microflex MALDIToF-MS using an a-cyano-4-hydroxycinnamic acid matrix (10 mg/ ml in H2O: MeCN:TFA, 50:47.5:2.5).

Table2. Peptide sequences and their molecular mass obtained by Maldi Mass Spectrometry.

peptide sequence	Maldi TOF MS
6- QYHQVLATHQ	1224.34
15- KFLYTAFAMQ	1219.45
22- NQTIWNHGNI	1196.29
31- QLQKWEDWVR	1386.58

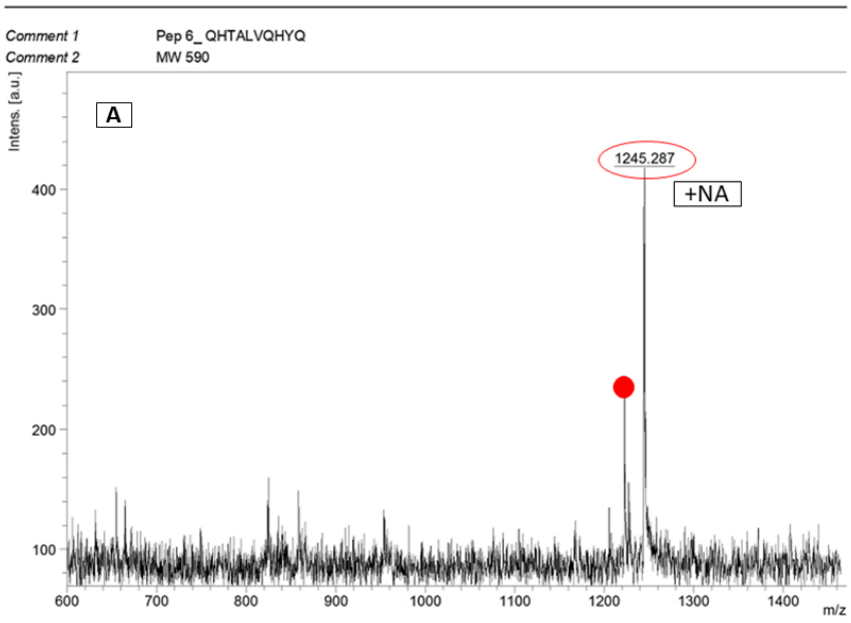

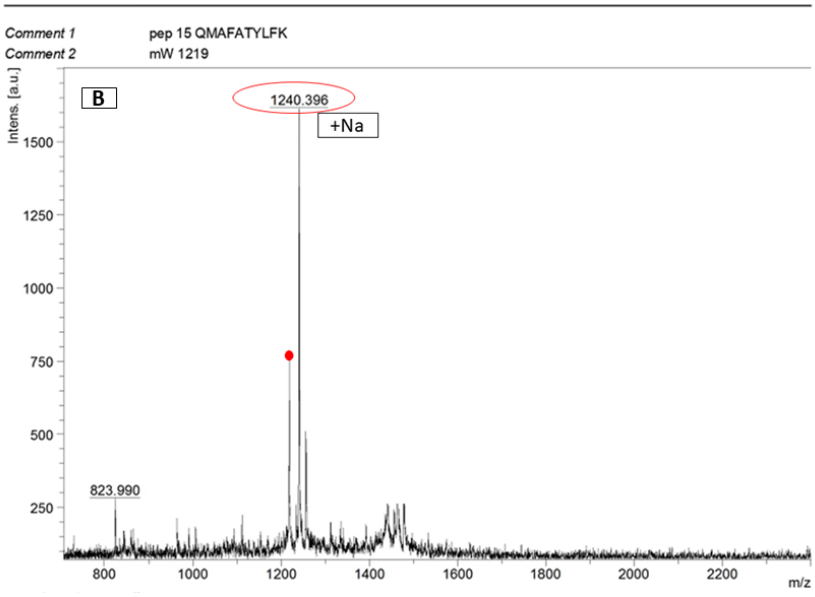
Comment 1
pep 15 QMAFATYLFK
Comment 2
mW 1219
B
1240.396
+Na
823.990
Intens. [a.u.]
1500
1250
1000
750
500
250
800
1000
1200
1400
1600
1800
2000
2200
m/z

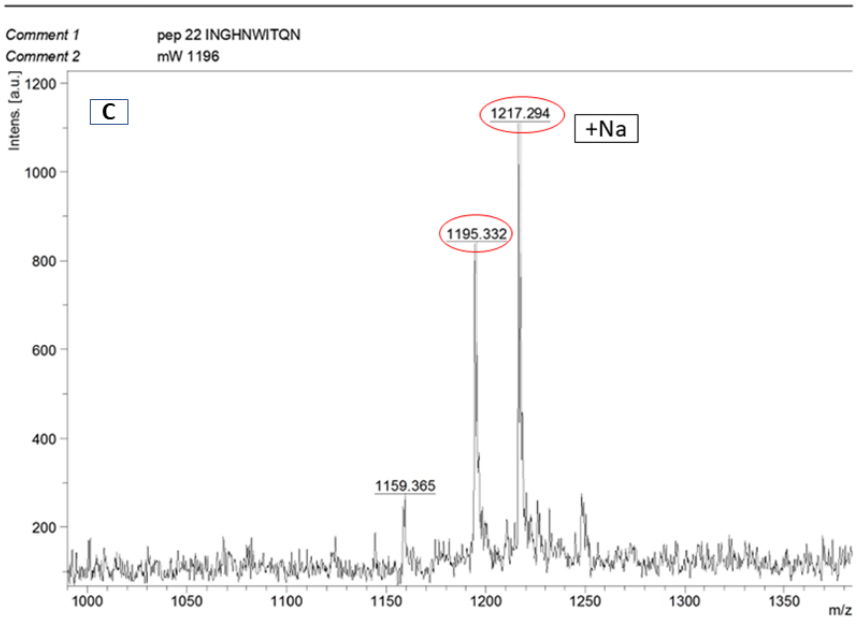
Comment 1
pep 22 INGHNWITQN
Comment 2
mW 1196
C
1217.294
+Na
1195.332
1159.365
Intens. [a.u.]
1200
1000
800
600
400
200
1000
1050
1100
1150
1200
1250
1300
1350
m/z

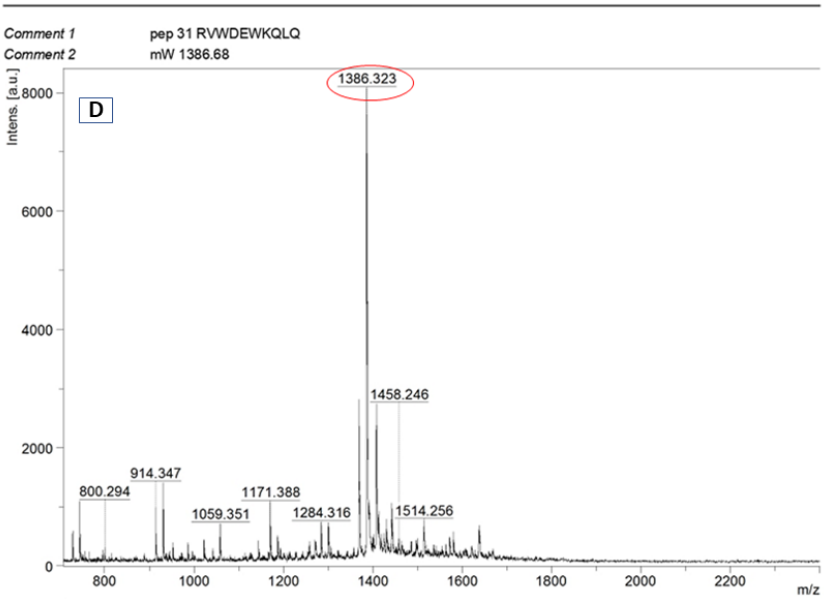

Figure 8: MS spectra of peptides 6 (**A**), 15 (**B**), 22 (**C**), and 31(**D**) on a Bruker Microflex MALDI-TOF-MS, using an a-cyano-4-hydroxycinnamic acid matrix.

4.3.3.3 Circular dichroism conformational analysis

To have preliminary information on the conformation of the synthesized peptides, CD experiments were recorded in pure water, in micelle solution composed of different SDS amounts, and in HFIP/water 50:50. The resulting CD spectra were used to estimate the secondary structure using the CDSSTR algorithm from the DICHROWEB website [23] (**Table 3**). Quantitative analysis of CD spectra indicates that peptides **6, 15,** and **22** increase the content of helical structures by increasing the content of SDS; on the contrary, peptide **31** conserved stable secondary structure at different SDS concentrations.

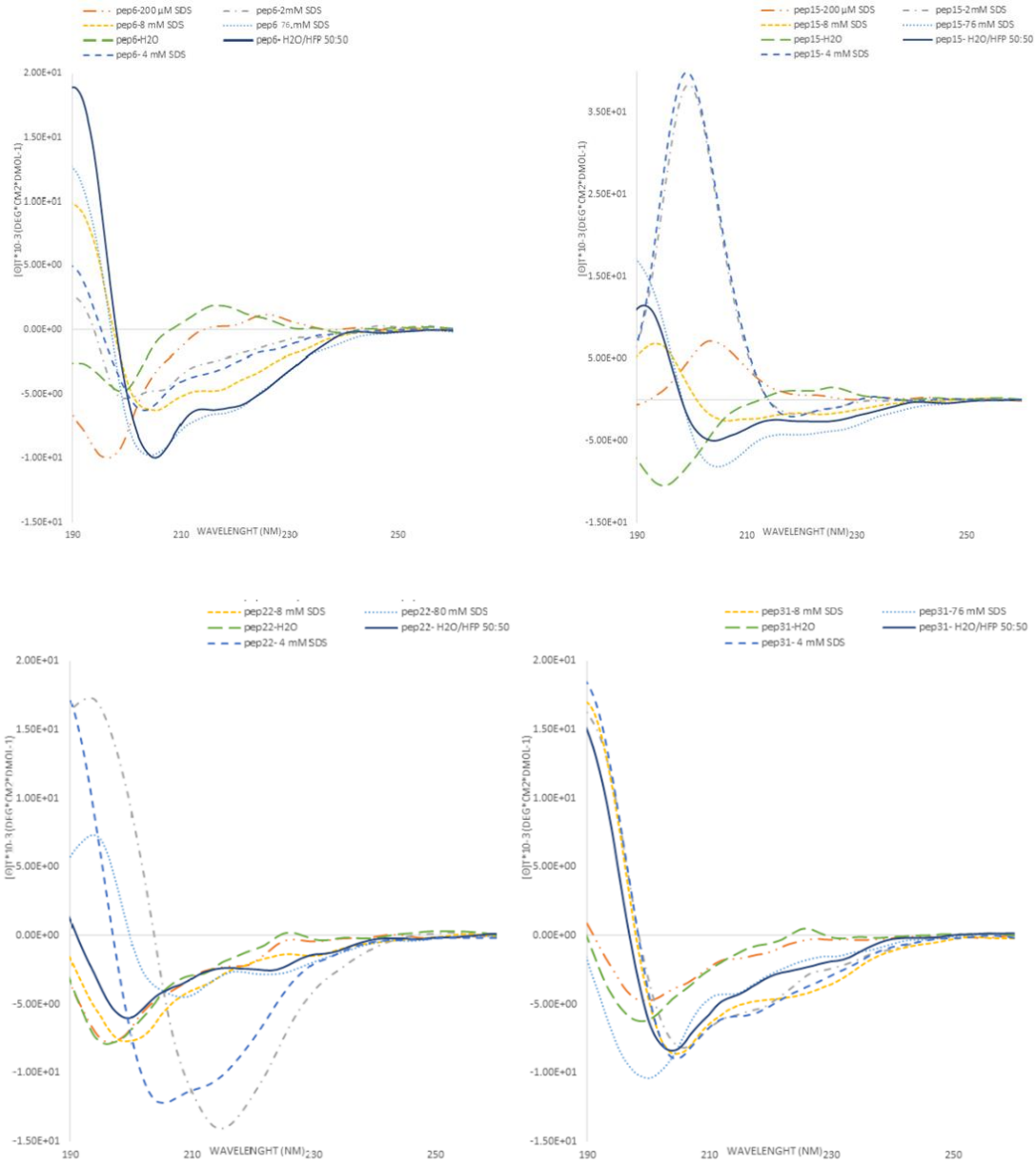

Figure 9. CD spectra of peptides (**6, 15, 22, 31**) recorded in different SDS concentration (200µM, 2mM, 4mM, 8mM, and 76mM) and HFIP/H_2O (50:50).

Table 3. secondary structure calculation by using the CDSSTR algorithm from the DICHROWEB website.

Pep6/SDS	%α-helix	%β-sheet	%Turns	%Random coil
Pep6-2mM SDS	6	29	15	50
Pep6-4mM SDS	28	22	18	43
Pep6-8mM SDS	39	15	17	29
Pep6-80mM SDS	53	16	12	19
Pep6-200MM SDS	0	15	7	76
Pep6-HFIP/H_2O	56	15	10	19
Pep6-H2O	1	43	21	36

Pep15/SDS	%α-helix	%β-sheet	%Turns	%Random coil
Pep15-2mM SDS	0	100	0	0
Pep15-4mM SDS	0	100	0	0
Pep15-8mM SDS	24	29	17	30
Pep15-80mM SDS	51	17	13	19
Pep15-200MM SDS	0	85.5	8	6.5
Pep15-HFIP/H_2O	43	25	12	22
Pep15/H2O	0	11	5.5	82.2

Pep22/SDS	%α-helix	%β-sheet	%Turns	%Random coil
Pep22-2mM SDS	57	21	7	15
Pep22-4mM SDS	51	26	8	15
Pep22-8mM SDS	6	13	12	69
Pep22-80mM SDS	47	20	16	17
Pep22-200MM SDS	0	27	12	56
Pep22-HFIP/H_2O	5	13	13	68
Pep22/H2O	0	22	13	63

Pep31/SDS	%α-helix	%β-sheet	%Turns	%Random coil
Pep31-2mM SDS	45	20	15	19
Pep31-4mM SDS	47	21	11	21
Pep31-8mM SDS	40	15	13	22
Pep31-80mM SDS	6	18	18	58
Pep31-200MM SDS	2	26	15	55
Pep31-HFIP/H_2O	23	29	19	29
Pep31/H2O	1	30	15	52

4.3.3.4 Peptide 31 Analogs

In recent years chemists have become increasingly successful in the design of peptide analogs that are resistant to metabolism while retaining high biological activity.[10]

Inspired by the peculiar conformational properties of **31** (**Table. 3**) we decided to synthesize 31 analogs by replacing the Trp residues included in its sequence with Phe and Ala residues as reported in **Table 4**.

We synthesized them like other peptides using TentaGel resin according to the standard SPPS protocol. The peptide was purified by preparative HPLC and confirmed the purity by analytical HPLC and MALDITof-MS (**Figure.10**).

Table 4. Analogs of peptide 31: sequences have been designed by replacing W residue with F and A amino acids.

Peptide	Sequence
31	QLQK**W**ED**W**VR
31.01	QLQK**F**EDWVR
31.02	QLQKWED**F**VR
31.03	QLQK**A**EDWVR
31.04	QLQKWED**A**VR

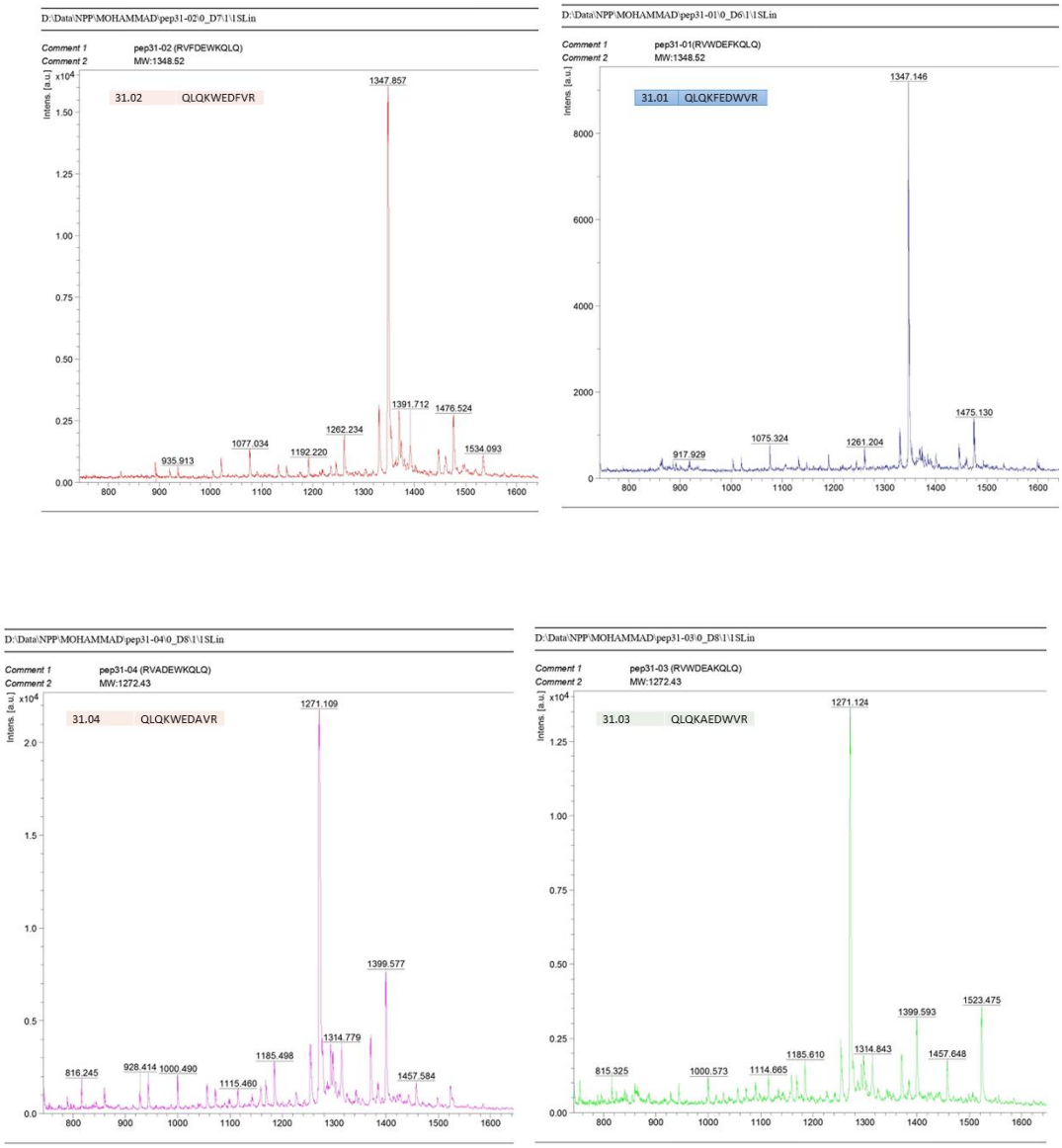

Figure. 10 The crude verification of peptides 31 analogs performed on a Bruker Microflex MALDIToF-MS using an a-cyano-4-hydroxycinnamic acid matrix.

4.4 Conclusions

The studies reported in the present chapter include the experiments performed at the Department of Drug Design and Pharmacology of the University of Copenhagen. During this period, I was mainly involved in synthetic experimental work to synthesize analogs of peptide C8. As data collected in our lab have previously demonstrated biological and biophysical

properties of C8 that are unique for a short peptide, with the intent of understanding the impact that could have stiffening of C8 structure on its properties, we synthesized a head to tail cyclic version of this peptide. Moreover, we synthesized C8 analogs where the Trp residues, which are critical for its biological activity, are replaced by Tryptamine residues.

In addition, with the intent of identifying new peptides that analogously to C8 could prevent FIV infection by preventing virus entry, we performed an epitope map scanning of the Gp36 sequence. Accordingly, four peptide sequences were selected to be synthesized, and among these, peptide 31, showing optimal conformational properties in SDS micelles, was chosen to be subjected to further structure activity relationship study.

4.5 Materials and Method

4.5.1- Peptide Synthesis

Linear peptides were synthesized using solid-phase peptide synthesis (SPPS) and Fmoc chemistry. After the swelling the resin, then followed by Fmoc deprotection by 20% piperidine in DMF for 3 × 4min. The resin was washed with DMF (10× 20s with 2 mL). Fmoc-protected amino acids were dissolved in DMF together with HOAt (both at a concentration of 0.4 M); they were then activated by the sequential addition of HATU (0.4 M in DMF) and of DIEA, and the mixture was immediately transferred into the reactor. Before and after the piperidine deprotection procedure, the resin was washed with DMF (3x). After the last deprotection cycle for the N-terminal amino acid, the resin was additionally washed with EtOH (5x) and dried in vacuo. Cleavage of the fully protected peptide acid from the solid support was performed with a Cleavage cocktail solution contain TFA/H_2O/TIS (95: 2.5: 2.5, 3 mL) solution for 2 h. The cleavage solution was collected and concentrated down to ~300 µl with a gentle stream of N2, then the peptide was precipitated and washed with diethyl ether (Et2O) (3x). After spontaneous evaporation of the residual Et2O, the peptides were additionally dried in vacuo overnight to remove excesses of AcOH and other volatile substances.

4.5.2 CD analysis

CD spectra were recorded at room temperature on a 815-Jasco spectropolarimeter, using a quartz cuvette with a path length of 0.1 cm. CD spectra of peptides (Pep6, Pep15, Pep22, Pep31) were acquired in H_2O, HFIP/H_2O (50:50) and in the presence of different concentrations of sodium dodecyl sulfate (SDS). The spectra are an average of three consecutive scans from 260 to 180 nm, recorded with a bandwidth of 1.0 nm, a D. I. T. of 4s. and a scan rate of 50 nm min^{-1}.

Figure 9 shows CD spectra were collected at 82µM SDS concentration for Pep6, Pep15, and Pep22 and 72 µM SDS concentration for Pep31 and the SDS at concentrations 200µM, 2mM, 4mM, 8mM, and 76mM and HFIP/H2O (50:50). The data were treated with the Savitzky–Golay smoothing procedure using 11 points in the Jasco Spectra Analysis software.[4, 24]

4.5.3 Synthesis of C8 peptoid (reach in indole ring)

The peptoid was synthesized manually (100mg scale) in disposable 5mL polypropylene reactors fitted with a PTFE filter. We used TentaGel S RAM resin 200 gram (0.23 mmol/g). The resin was swelled in DMF for 2 h at room temperature, followed by Fmoc deprotection by 20% piperidine in DMF for 3 × 4min. The resin was washed with DMF (10× 20s with 2 mL). The acylation step was performed using 0.6M bromoacetic acid in DMF (0.210 g of bromoacetic acid in 2.5 ml of DMF) and 3.2M DIC (500 µLof DIC in 500 µL DMF) for 20min (30min for first acylation step). Displacement was achieved through the addition of 1M Tryptamine in DMF for 1 h (generally 20min for tryptamine) at room temperature. then in continue for the coupling of the other amino acids we used Fmoc/*t*Bu amino acid like normal synthesis procedure. Then after the synthesis we used cleavage cocktail (TFA: DCM: anisole, 49:49:2) for 30min, shaking at room temperature (**Figure 2**). After cleavage, the cleavage cocktail solution was filtered and evaporated under N2 gas. The residual was dissolved in 5%

acetonitrile in milli-Q water. Then C8 peptoid was analyzed using analytical HPLC by C18 Luna 150 × 4.6mm 100 Å column, flow rate o.1 ml/min and standard HPLC C18 Xbridge 10 × 250 mm 130 Å column, 24◦C, in 20- 100 % of B, which solvent A 100 %water (0.1% TFA) solvent B was 90 % acetonitrile (0.1% TFA), flow rate 5 mL/min (**Figure 3**).

Follow in purification done by using preparative HPLC which done on a C-18 column using 0.1 % aqueous TFA as a buffer A and CH_3CN/H_2O (90:10) with 0.1% TFA as buffer B. then at the end the prep product confirmed by MALDI ToF-MS (**Figure 3**), and control of purities was done by using MALDI Tof/MS (**Figure 4**).

4.5.4 Cyclic Peptide Synthesis

To eliminate epimerization, tryptophane has been used as the C-terminus of the linear precursor . The Cyclic C8 was synthesized via standard SPPS on 2- chlorotrityl resin and The linear peptide was assembled by using Fmoc/tBu protocol but also for Tryptophane residues, we used Fmoc-Trp(Boc)-OH and after the synthesis the linear peptide released in weak acidic conditions (2%TFA/DCM). (**Figure 1**).

H-Gly-2-chlorotritil resin of loading 1.6mmol/g (300mg) was pre-activate and swelled with DMF for 2h; then couplings were achieved with Fmoc-amino acid: HOAT, HBTU, and DIPEA (4: 4: 8 equiv.) using DMF (2.5 mL) as the solvent followed by thorough washings with DCM and DMF (10 mL, 4x each). solution was adjusted to a basic pH = 8 and stirred overnight at 25 °C.

TFA and DCM were evaporated and the residual DMF layer was highly diluted using DCM(50ml), which was used for cyclization. The fully protected peptide (Alloc removed) (0.025 mmol, 1 equiv.) and a solution of HOAt (62 mg, 0.456 mmol, 4equiv.) in a minimum amount of DMF (0.3 mL) were dissolved in DCM (50 mL) followed by the addition of PyAOP (475.5 mg, 0.456 mmol, 4 equiv.) and DIPEA(317µL, 0.456 mmol, 8equiv.). The solution was

adjusted to a basic pH = 8 and stirred overnight at 25 °C. The cyclization was monitored by Q-TOF MS. the DCM was evaporated completely, and water was added to the residual DMF solution. The precipitate formed was centrifuged, lyophilized and treated with 2 mL of TFA : H_2O (95 : 5) for 90 min at room temperature. To this was added cold diethyl ether to precipitate the peptide, that was once again washed with ether, centrifuged and dissolved the peptide in water. The crude peptide was subjected to semi-preparative HPLC and the fractions with purity >95% were pooled and lyophilized. The pure peptide was analyzed by analytical HPLC and Q-TOF MS.(**Figure 11**).

4.6 References

1. Wild, C.T., et al., Peptides corresponding to a predictive alpha-helical domain of human immunodeficiency virus type 1 gp41 are potent inhibitors of virus infection. 1994. **91**(21): p. 9770-9774.
2. Scrima, M., et al., Structural features of the C8 antiviral peptide in a membrane-mimicking environment. Biochim Biophys Acta, 2014. **1838**(3): p. 1010-8.
3. Di Marino, D., et al., Binding of the Anti-FIV Peptide C8 to Differently Charged Membrane Models: From First Docking to Membrane Tubulation. Front Chem, 2020. **8**: p. 493.
4. Grimaldi, M., et al., Structural basis of antiviral activity of peptides from MPER of FIV gp36. PLoS One, 2018. **13**(9): p. e0204042.
5. D'Errico, G., et al., Interaction of short modified peptides deriving from glycoprotein gp36 of feline immunodeficiency virus with phospholipid membranes. Eur Biophys J, 2009. **38**(7): p. 873-82.
6. Giannecchini, S., et al., Antiviral activity and conformational features of an octapeptide derived from the membrane-proximal ectodomain of the feline immunodeficiency virus transmembrane glycoprotein. 2003. **77**(6): p. 3724-3733.
7. D'Ursi, A.M., et al., Development of antiviral fusion inhibitors: short modified peptides derived from the transmembrane glycoprotein of feline immunodeficiency virus. Chembiochem, 2006. **7**(5): p. 774-9.
8. Loffet, A.J.J.o.p.s.a.o.p.o.t.E.P.S., Peptides as drugs: is there a market? 2002. **8**(1): p. 1-7.
9. Joo, S.H., Cyclic peptides as therapeutic agents and biochemical tools. Biomol Ther (Seoul), 2012. **20**(1): p. 19-26.
10. Veber, D.F. and R.M.J.T.i.N. Freidinger, The design of metabolically-stable peptide analogs. 1985. **8**: p. 392-396.
11. Roxin, Á. and G. Zheng, Flexible or fixed: a comparative review of linear and cyclic cancer-targeting peptides. Future Med Chem, 2012. **4**(12): p. 1601-18.
12. Choi, J.S. and S.H. Joo, Recent Trends in Cyclic Peptides as Therapeutic Agents and Biochemical Tools. Biomol Ther (Seoul), 2020. **28**(1): p. 18-24.
13. Horton, D.A., G.T. Bourne, and M.L. Smythe, Exploring privileged structures: the combinatorial synthesis of cyclic peptides. J Comput Aided Mol Des, 2002. **16**(5-6): p. 415-30.
14. Rezai, T., et al., Testing the conformational hypothesis of passive membrane permeability using synthetic cyclic peptide diastereomers. J Am Chem Soc, 2006. **128**(8): p. 2510-1.
15. Lone, A., et al., Synthesis of Peptoids Containing Multiple Nhtrp and Ntrp Residues: A Comparative Study of Resin, Cleavage Conditions and Submonomer Protection. Front Chem, 2020. **8**: p. 370.
16. Vogel, H.J., et al., Towards a structure-function analysis of bovine lactoferricin and related tryptophan- and arginine-containing peptides. Biochem Cell Biol, 2002. **80**(1): p. 49-63.
17. Kwon, Y.U. and T. Kodadek, Quantitative evaluation of the relative cell permeability of peptoids and peptides. J Am Chem Soc, 2007. **129**(6): p. 1508-9.
18. Reddy, M.M. and T. Kodadek, Protein "fingerprinting" in complex mixtures with peptoid microarrays. Proc Natl Acad Sci U S A, 2005. **102**(36): p. 12672-7.
19. Rantalainen, K., et al., Co-evolution of HIV envelope and apex-targeting neutralizing antibody lineage provides benchmarks for vaccine design. 2018. **23**(11): p. 3249-3261.
20. Abraham, M.J., et al., GROMACS: High performance molecular simulations through multi-level parallelism from laptops to supercomputers. 2015. **1**: p. 19-25.
21. Zhou, J. and K.J.A.p.l. Komvopoulos, Interfacial viscoelasticity of thin polymer films studied by nanoscale dynamic mechanical analysis. 2007. **90**(2): p. 021910.
22. D'Ursi, A.M., et al., Retroinverso analogue of the antiviral octapeptide C8 inhibits feline immunodeficiency virus in serum. 2003. **46**(10): p. 1807-1810.
23. Whitmore, L. and B.A. Wallace, DICHROWEB, an online server for protein secondary structure analyses from circular dichroism spectroscopic data. Nucleic Acids Res, 2004. **32**(Web Server issue): p. W668-73.
24. Giannecchini, S., et al., Antiviral activity and conformational features of an octapeptide derived from the membrane-proximal ectodomain of the feline immunodeficiency virus transmembrane glycoprotein. J Virol, 2003. **77**(6): p. 3724-33.
25. Oddo, A., Nyberg, N. T., Frimodt-Møller, N., Thulstrup, P. W., & Hansen, P. R. (2015). The

effect of glycine replacement with flexible ω-amino acids on the antimicrobial and haemolytic activity of an amphipathic cyclic heptapeptide. *European journal of medicinal chemistry*, *102*, 574-581.